A fungal member of the *Arabidopsis thaliana* phyllosphere antagonizes *Albugo laibachii* via a secreted lysozyme

Katharina Eitzen[1,2], Priyamedha Sengupta[1], Samuel Kroll[2], Eric Kemen*[2,3], Gunther Doehlemann*[1]

[1] *Institute for Plant Sciences and Cluster of Excellence on Plant Sciences (CEPLAS), University of Cologne, Center for Molecular Biosciences, Zuelpicher Str. 47a, 50674 Cologne, Germany.*

[2] *Max Planck Institute for Plant Breeding Research, Carl-von-Linne-Weg 10, 50829 Köln, Germany.*

[3] *Department of Microbial Interactions, IMIT/ZMBP, University of Tübingen, Tübingen, Germany.*

* correspondence to:

Eric Kemen, eric.kemen@uni-tuebingen.de,

Gunther Doehlemann, g.doehlemann@uni-koeln.de

Short title: Microbial antagonism suppressing *Albugo laibachii* infection

Key words: microbial antagonism, plant pathogen, *Albugo laibachii*, Ustilaginales, Arabidopsis, transcriptomics, effectors

Abstract

Plants are not only challenged by pathogenic organisms, but also colonized by commensal microbes. The network of interactions these microbes establish with their host and amongst each other is suggested to contribute to the immune responses of plants against pathogens. In wild *Arabidopsis thaliana* populations, the oomycete pathogen *Albugo laibachii* has been shown to play an influential role in structuring the leaf phyllosphere. We show that the epiphytic yeast *Moesziomyces bullatus* ex *Albugo* on *Arabidopsis,* a close relative of pathogenic smut fungi, is an antagonistic member of the *A. thaliana* phyllosphere, which reduces infection of *A. thaliana* by *A. laibachii*. Combination of transcriptome analysis, reverse genetics and protein characterization identified a GH25 hydrolase with lysozyme activity as the major effector of this microbial antagonism. Our findings broaden the understanding of microbial interactions within the phyllosphere, provide insights into the evolution of epiphytic basidiomycete yeasts and pave the way for the development of novel biocontrol strategies.

Introduction

Plants are colonized by a wide range of microorganisms. While some microbes enter the plant and establish endophytic interactions with a broad range of outcomes from beneficial to pathogenic, plant surfaces harbor a large variety of microbial organisms. Recent research has focused largely on the importance of the rhizosphere microbiota in nutrient acquisition, protection from pathogens, and boosting overall plant growth and development (1–3). However, the above ground parts of the plant including the phyllosphere are colonized by diverse groups of microbes that also assist in plant protection and immunity (4,5). The environment has a major impact on the microbial communities of the leaf surface, ultimately influencing their interactions with the host (6).

Scale-free network analysis was performed with the leaf microbial population of *Arabidopsis thaliana* (7). The majority of the interactions between kingdoms, e.g. fungi and bacteria, were found to be negative, consistent with the fact that rather the antagonistic interactions stabilize a microbial community (8). Phyllosphere network analysis of *A. thaliana* identified a small number of microbes as “hub” organisms, i.e.

influential microbes which have severe effects on the community structure. The major hub microbe in the *A. thaliana* phyllosphere is the oomycete *Albugo laibachii*, which is a pathogenic symbiont biotrophic of *Arabidopsis* (7). This pathogen has been shown to significantly reduce the bacterial diversity of epiphytic and endophytic leaf habitats. Since bacteria generally comprise a large proportion of the phyllosphere microbiome (9), phylogenetic profiling of *A. thaliana* was also directed towards identifying a small group of bacteria that frequently colonize *A. thaliana* leaves. The analysis helped to develop a synthetic community of bacteria for experiments in gnotobiotic plants.

Besides bacteria and oomycetes, the microbiota of the *A. thaliana* leaf also comprises a broad range of fungi. Among those fungi, basidiomycete yeasts are frequently found and the most frequent ones are the epiphytic basidiomycete genus *Dioszegia* (7), as well as an anamorphic yeast associated with *A. laibachii* infection, classified as *Pseudozyma. sp.* and belonging to Ustilaginales. This order includes many pathogens of important crop plants, for example corn smut and loose smut of oats, barley and wheat are caused by *Ustilago maydis*, *U. avenae*, *U. nuda* and *U. tritici*, respectively. Generally, pathogenic development of smut fungi is linked with sexual recombination and plant infection is only initiated upon mating when two haploid sporidia form a dikaryotic filament (10). Ustilaginales *Pseudozyma* sp. yeasts, however, are not known to be pathogenic. While they are found in anamorphic stage, they epiphytically colonize a wide range of habitats via where an infrequent sexual recombination might occur (11). Phylogenetic reconstruction (12) showed that the smut pathogen of millet, *Moesziomyces bullatus* and four species of *Pseudozyma*, namely *P. antarctica*, *P. aphidis*, *P. parantarctica* and *P. rugulosa* form a monophyletic group. The latter does represent anamorphic and culturable stages of *M. bullatus* and, hence, can be grouped to this genus. *Moesziomyces* strains have been reported in a number of cases to act as microbial antagonists. A strain formerly classified as *Pseudozyma aphidis* (now *Moesziomyces bullatus*) inhibited *Xanthomonas campestris* pv. *vesicatoria*, *X. campestris* pv. *campestris*, *Pseudomonas syringae* pv. *tomato*, *Clavibacter michiganensis*, *Erwinia amylovora*, and *Agrobacterium tumefaciens in-vitro* and also led to the activation of induced defense responses in tomato against the pathogen (13). It was reported that *P. aphidis* can parasitize the hyphae and spores of

Podosphaera xanthii (14). *Pseudozyma churashimaensis* was reported to induce systemic defense in pepper plants against *X. axonopodis*, Cucumber mosaic virus, Pepper mottle virus, Pepper mild mottle virus, and broad bean wilt virus (15).

In the present study, we explored the antagonistic potential of an anamorphic Ustilaginales yeast within the leaf microbial community of *A. thaliana*. We show that *Moesziomyces bullatus* ex *Albugo* on *Arabidopsis* (which will be referred to as MbA, from further on in this paper) prevents infection by the oomycete pathogen *A. laibachii* and identified fungal candidate genes that were upregulated in the presence of *A. laibachii*, when both the microbes were co-inoculated in the host plant. A knockout mutant of one of the candidates, which belongs to the glycoside hydrolase – family 25 (GH25), was found to lose its antagonistic abilities towards *A. laibachii,* providing mechanistic insights into fungal-oomycete antagonism within the phyllosphere microbiota. Functional characterization of GH25 will be an important step towards establishing *MbA* as a suitable biocontrol agent.

Results

In a previous study we isolated a basidiomycetous yeast from *Arabidopsis thaliana* leaves infected with the causal agent of white rust, *Albugo laibachii* (7). This yeast was tightly associated with *A. laibachii* spore propagation. Even after years of subculturing in the lab and re-inoculation of plants with frozen stocks of *A. laibachii* isolate Nc14, this yeast remained highly abundant in spore isolates. Phylogenetic analyses based on fungal ITS-sequencing identified the yeast as *Pseudozyma sp*. Those yeasts can be found across the family of Ustilaginaceae, being closely related to pathogens of monocots like maize, barley, sugarcane or sorghum (Figure 1A and (16)). Microscopic analyses verified the morphological similarity between the putative *Pseudozyma sp*. and the Ustilaginaceous pathogen *Ustilago maydis*, the causal agent of corn smut (Figure 1B; (16)). Based on phylogenetic similarity to the pathogenic smut *Moesziomyces bullatus* which infects millet, several anamorphic *Pseudozyma* isolates were suggested to be renamed and grouped to *M. bullatus* (12). Since the *Pseudozyma sp*. that was isolated from *A. laibachii* spores groups into the same cluster, we classified

this newly identified species as *MbA (Moesziomyces bullatus* ex *Albugo* on *Arabidopsis*).

Based on the identification of *MbA* as heaving a significant effect on bacterial diversity in the *Arabidopsis* phyllosphere, we tested its interaction with 30 bacterial strains from 17 different species of a synthetic bacterial community (SynCom, Table S1) of *Arabidopsis* leaves in one-to-one plate assays. This experiment identified seven strains being inhibited by *Moesziomyces,* as indicated by halo formation after 7 days of co-cultivation (Supplementary Figure S1). Interestingly, this inhibition was not seen when the pathogenic smut fungus *U. maydis* was co-cultivated with the bacteria, indicating a specific inhibition of the bacteria by *MbA* (Supplementary Figure S1).

The primary hub microbe in the *Arabidopsis* phyllosphere was found to be the pathogenic oomycete *A. laibachii,* which was isolated in direct association with *Moesziomyces* (7). To test if both species interfere with each other, we deployed a gnotobiotic plate system and quantified *A. laibachii* infection symptoms on *Arabidopsis*. In control experiments, spray inoculation of only *A. laibachii* spores on *Arabidopsis* leaves led to about 33% infected leaves at 14 dpi (Figure 2). When the bacterial SynCom was pre-inoculated on leaves two days before *A. laibachii* spores a significant reduction of *A. laibachii* infection by about 50% was observed (Figure 2). However, if *Moesziomyces* was pre-inoculated with the bacterial SynCom, *A. laibachii* spore production was almost completely abolished. Similarly, the pre-inoculation of only *MbA* resulted in an almost complete loss of *A. laibachii* infection, independently of the presence of a bacterial community (Figure 2). The antagonistic effect of *MbA* towards *A. laibachii* was further confirmed using Trypan blue staining of *A. laibachii* infected *A. thaliana* leaves. *A. laibachii* forms long, branching filaments on *Arabidopsis* leaves at 15 dpi. Contrary, in presence of *MbA*, we observed mostly zoospores forming either no or very short hyphae, while further colonization of the leaf with long, branching was not observed (Supplementary figure S2B). Together, of findings demonstrates that *MbA* holds a strong antagonistic activity towards *A. laibachii*, resulting in efficient biocontrol of pathogen infection. Thus, *MbA* is an important member of the *A. thaliana* phyllosphere

148 microbial community. However, despite, several reports of the basidiomycete yeasts
149 acting as antagonists, genomic analysis of the said group is rather limited. We therefore
150 sequenced the genome of *MbA* and established molecular tools allowing functional
151 genetic approaches.

152

153 **The genome of *MbA.***

154 Genome sequence of *MbA* was analyzed by Single Molecule Real-Time sequencing
155 (Pacific Biosciences, Menlo Park, CA), which lead to 69674 mapped reads with an
156 accuracy of 87.3% and 8596bp sub-read length. Sequence assembly using the HGAP-
157 pipeline (Pacific Biosciences) resulted in 31 Contigs with a N_{50}Contig Length of 705kb.
158 The total length of all contigs results in a predicted genome size of 18.3Mb (Table 1).
159 Gene prediction for the *MbA* genome with Augustus (17) identified 6653 protein coding
160 genes, of which 559 carry a secretion signal. Out of these 559, 380 are predicted to be
161 secreted extracellularly (i.e. they do not carry membrane domains or cell-wall anchors)
162 (Table 1). The small genome size and high number of coding genes results in a highly
163 compact genome structure with only small intergenic regions. These are features
164 similarly found in several pathogenic smut fungi such as *U. maydis* and *S. reilianum*
165 (Table 1). Remarkably, both *MbA* and *Anthracocystis flocculosa,* which is another
166 anamorphic and apathogenic yeast, show a similarly high rate of introns, while the
167 pathogenic smut fungi have a significantly lower intron frequency (Table 1).

168 To gain better insight in the genome organization of *MbA,* we compared its structure
169 with the *U. maydis* genome, which serves as a manually annotated high-quality
170 reference genome for smut fungi (18). Out of the 31 *MbA* contigs, 21 show telomeric
171 structures and a high synteny to chromosomes of *U. maydis,* with three of them
172 displaying major events of chromosomal recombination (Figure 3A). Interestingly, the
173 *Moesziomyces* contig 2, on which also homologs to pathogenic loci like the *U. maydis*
174 virulence cluster 2A (18) can be found, contains parts of three different *U. maydis*
175 chromosomes (Chr. 2, 5, 20) (Supplementary figure S3). The second recombination
176 event on contig 6 affects the *U. maydis* leaf-specific virulence factor *see1*, which is
177 required for tumor formation (19). This recombination event is also found in the genome

of the maize head smut *S. reilianum*, wherein the *U. maydis* chromosomes 5 and 20 recombined in the promoter region of the *see1* gene (Figure 3B). In this respect it should be noted that *S. reilianum*, although infecting the same host, does not produce leaf tumors as *U. maydis* does (20).

Also the third major recombination event, affecting *MbA* contig 8, changes the genomic context genes encoding essential virulence factors in *U. maydis* (*stp1* & *pit1/2*), as well as the A mating type locus, which is important for pheromone perception and recognition of mating partners (21). Based on the strong antibiotic activities of *MbA,* we mined the genome of *MbA* for the presence of secondary metabolite gene clusters. Using AntiSMASH, we were able to predict 13 of such clusters, of which three can be assigned to terpene synthesis, three contain non-ribosomal peptide synthases and one cluster has a polyketide synthetase as backbone genes (Supplementary Figure S4A). Interestingly, the secondary metabolite cluster that is involved in the production of the antimicrobial metabolite ustilagic acid in other Ustilaginomycetes, is absent in *MbA* (Supplementary Figure S4B). On the contrary, we could identify three *MbA* specific metabolite clusters which could potentially be involved in the antibacterial activity of *MbA* (Supplementary Figure S4C).

A previous genome comparison of the related Ustilaginales yeast *A. flocculosa* with *U. maydis* concluded that this anamorphic strain had lost most of its effector genes, reflecting the absence of a pathogenic stage in this organism (22). In contrast, *MbA* contains 1:1 homologs of several known effectors with a known virulence function in *U. maydis* (Table 2). We previously found that *Moesziomyces* sp. possess functional homologues of the *pep1* gene, a core virulence effector of *U. maydis* (23), suggesting that such anamorphic yeasts have the potential to form infectious filamentous structures by means of sexual reproduction (11). To assess the potential virulence activity of *MbA* effector homologs, we expressed the homolog of the *U. maydis* core effector Pep1 in an *U. maydis pep1* deletion strain (SG200Δ01987). This resulted in complete restoration of *U. maydis* virulence, demonstrating that, when ectopically expressed, *MbApep1* encodes a functional effector (Supplementary Figure S5).

A hallmark of the *U. maydis* genome structure is the presence of large clusters with effector genes, the expression of which is only induced during plant infection (18). To assess the presence of potential virulence clusters in *MbA*, we compared all *U. maydis* effector gene clusters to the *MbA* genome, based on homology. This revealed that the twelve major effector clusters of *U. maydis* are present in *MbA.* However, while many of the clustered effector genes are duplicated in pathogenic smut fungi, *MbA* carries only a single copy of each effector gene. This results in the presence of "short" versions of the *U. maydis* gene effector clusters (Supplementary Figure S6). This gets particularly obvious for the biggest and most intensively studied virulence cluster of smut fungi, the effector cluster 19A (20,24,25). In *MbA* only three out of the 24 effector genes present in *U. maydis* are conserved in this cluster (Figure 4). Interestingly, some anamorphic yeasts like *Kalmanozyma brasiliensis* and *A. flocculosa* completely lost virulence clusters, while another non-pathogenic member of the Ustilaginales, *Pseudozyma hubeiensis,* shows an almost complete set of effectors when compared to *U. maydis* (Figure 4).

Genetic characterization of *MbA*

To perform reverse genetics in *MbA,* we established a genetic transformation system based on protoplast preparation and PEG-mediated DNA transfer. In preliminary transformation assays, we expressed a cytosolic GFP reporter-gene under control of the constitutive *o2tef*-Promoter (Figure 5A). For the generation of knockout strains, a split marker approach was used to avoid ectopic integrations (Figure 5B). To allow generation of multiple knockouts, we used a selection marker-recycling system (pFLPexpC) which allows selection marker excision at each transformation round (26).

We decided to apply the transformation system to study the *MbA* mating type loci in more detail. Although phylogenetically closely related to *U. hordei,* which has a bi-polar mating system, *MbA* owns a tetrapolar mating system whereby both mating type loci are physically not linked. This situation is similar to the mating type structure in the pathogenic smut *U. maydis* (Figure 5A). The *a*-locus, which encodes a pheromone – receptor system that is required for sensing and fusion of compatible cells, is located on

237 contig 6. The *b*-locus can be found on contig 1. This multiallelic mating locus contains
238 two genes (*b-East* and *b-West*), which code for a pair of homeodomain transcription
239 factors. Upon mating of compatible cells, pathogenic and sexual development are
240 triggered by a heterodimeric bE/bW complex (10). Since the *MbA* genome is completely
241 equipped with mating type genes, we first deployed a screen for potential mating
242 partners. To this end, we screened wild *M. bullatus* isolates to find a suitable mating
243 partner, but we could not observe any mating event (Supplementary Figure S7). To test
244 if *MbA* is able to undergo pathogenic differentiation in the absence of mating, we
245 generated a self-compatible strain (CB1) which carries compatible b-mating alleles: to
246 construct the CB1 strain, we used compatible alleles of the *b-East* and *b-West* genes of
247 the barley smut *U. hordei*, a pathogen which is the phylogenetically most closely related
248 to *MbA* and amenable to reverse genetics. The native *MbA* locus was replaced by the
249 compatible *U. hordei b-East* and *b-West* gene alleles via homologous recombination
250 (Figure 6B).

251 Incubation of the *MbA* CB1 on charcoal plates led to the formation of aerial hyphae with
252 the characteristic fluffy phenotype of filamentous strains like the self-compatible,
253 solopathogenic *U. maydis* SG200 strain (Figure 6C). A second established method to
254 induce filament formation in smuts is on hydrophobic parafilm (27). Quantification after
255 18 hours incubation of *MbA* CB1 on parafilm resulted in the formation of filaments
256 comparable to those of the *U. maydis* SG200 strain (Figure 6D). While about 17% of
257 *MbA* wild type cells showed filaments, the CB1 strain with compatible b-genes showed
258 38% filamentous growth.
259 Formation of appressoria is a hallmark of pathogenic development in smut fungi (27).
260 While the switch from yeast-like growth to filamentous development is the first step in
261 the pathogenic development of smut fungi, host penetration is accompanied by the
262 formation of a terminal swelling of infectious hyphae, termed “appressoria”. Induction of
263 appressoria-formation *in vitro* can be induced by adding 100 µM of the cutin monomer
264 16-Hydroxyhexadecanoic acid (HDD) to the fungal cells prior to cell spraying onto a
265 hydrophobic surface (27). In absence of HDD, only about 8% of the *U. maydis* SG200
266 cells and 14% of the *MbA* cells formed appressoria on parafilm 24 hours after spraying
267 (Figure 6E). Addition of 100µM HDD resulted in a significant induction of appressoria in

both *U. maydis* and *MbA*, demonstrating that *MbA* does hold the genetic repertoire to form infection structures *in-vitro*. Together, the analysis of the recombinant CB1 strain indicates that *MbA* can sense pathogenesis-related surface cues and produce penetration structures to a similar level as that seen for the pathogenic model organism *U. maydis.*

Identification of microbe-microbe effector genes by RNA-Seq

To study the transcriptomic response of *MbA* to different biotic interactions, RNA sequencing was performed. The *MbA* transcriptome was profiled in five different conditions (Figure 7A; cells in axenic culture versus cells on-planta, on-planta + SynCom, on-planta + *A. laibachii*, on-planta + SynCom + *A. laibachii*). Inoculations of *A. thaliana* leaves were performed as described above for *A. laibachii* infection assays (Figure 7A). For *MbA* RNA preparation, the epiphytic microbes were peeled from the plant tissue by using liquid latex (see methods section for details).

The libraries of the 15 samples (five conditions in three biological replicates each) were generated by using a poly-A enrichment and sequenced on an Illumina HiSeq4000 platform. The paired end reads were mapped to the *MbA* genome by using Tophat2 (28). The analysis revealed that *MbA* cells on *A. thaliana* leaves (on-planta) downregulated 1300 and upregulated 1580 genes compared to cells in axenic culture (Figure 7B). Differentially expressed genes were determined with the "limma"-package in R on "voom" (Supplementary Figure S8) using a False discovery rate threshold of 0.05 and log2FC > 0. A GO-terms analysis revealed that, among the downregulated genes, 50% were associated with primary metabolism (Supplementary Figure S9). In the two conditions in which *A. laibachii* was present, we observed upregulation of 801 genes. Among these genes, 411 genes were specific to co-incubation of *MbA* with *A. laibachii* and SynCom while 174 were specific to incubation with *A. laibachii* only. A set of 216 genes was shared in both conditions (Figure 7B).

In presence of *A. laibachii,* mainly metabolism- and translation-dependent genes were upregulated, which might indicate that *MbA* can access a new nutrient source in presence of *A. laibachii* (Supplementary Figure S9). Among all *A. laibachii* – induced *MbA* genes, 25 genes encode proteins carrying a secretion signal peptide and having

no predicted transmembrane domain (Figure 7C). After excluding proteins being predicted to be located in intracellular organelles, nine candidate genes remained as potential microbe-microbe dependent effectors, i.e. *MbA* genes which are induced by *A. laibachii*, show no or low expression in axenic culture and encode for putative secreted proteins (Figure 7C). Interestingly, four of these genes encode putative glycoside hydrolases. Furthermore, two genes encode putative peptidases, one gene likely encodes an alkaline phosphatase and two encode uncharacterized proteins (Figure 7C).

To directly test the eventual antagonistic function of those genes towards *A. laibachii*, we selected the two predicted glycoside hydrolases-encoding genes *g5* & *g2490* (GH43 & GH25) and the gene encoding the uncharacterized protein *g5755* for gene deletion in *MbA.* The respective mutant strains were tested in stress assays to assess, whether the gene deletions resulted in general growth defects. Wild type and mutant *MbA* strains were exposed to different stress conditions including osmotic stress (sorbitol, NaCl), cell wall stress (calcofluor, congored) and oxidative stress (H_2O_2). Overall, in none of the tested conditions we observed a growth defect of the deletion mutants in comparison to wild type *MbA* (Supplementary Figure S10). To test an eventual impact of the deleted genes in the antagonism of the two microbes, the *MbA* deletion strains were each pre-inoculated on *A. thaliana* leaves prior to *A. laibachii* infection. Deletion of *g5* resulted in a significant but yet marginal increase of *A. laibachii* disease symptoms, while deletion of *g5755* had no effect on *A. laibachii*. We therefore considered these two genes being not important for the antagonism of *MbA* towards *A. laibachii.* Strikingly, the *MbA Δg2490* strain almost completely lost its biocontrol activity towards *A. laibachii.* This phenotype was reproduced by two independents *g2490* deletion strains (Figure 8A). To check if this dramatic loss of microbial antagonism is specific to the deletion of *g2490*, in-locus genetic complementation of strain *Δg2490_1* was performed via homologous recombination. The resulting strain *MbA Δg2490/compl* regained the ability to suppress *A. laibachii* infection, confirming that the observed phenotype specifically resulted from the deletion of the *g2490* gene (Figure 8B). Together, these results demonstrate that the biocontrol of the pathogenic oomycete *A. laibachii* by the basidiomycete yeast *MbA* is determined by the secretion of a previously

uncharacterized GH25 enzyme, which is transcriptionally activated specifically when both microbes are co-colonizing the *A. thaliana* leaf surface.

Functional characterization of the secreted MbA hydrolase

To characterize the protein function of the GH25 encoded by *MbA g2490*, we were using *Pichia pastoris* for heterologous expression. The recombinant protein was tagged with polyhistidine tag for Ni-NTA affinity purification. The purified protein was detected at an expected size of 27kDa (Supplementary Figure S11A). In addition, via site directed mutagenesis a mutated version of the protein was generated, carrying a single amino exchange at the predicted active site (GH25_D124E). Both active and mutated versions of the GH25 hydrolase were subjected to a quantitative lysozyme activity assay using fluorogenic substrate *Micrococcus lysodeikticus* with commercial Hen egg-white lysozyme as a control. We noticed a concentration dependent increase in relative fluorescence unit (RFU)/min for the active GH25 in molar concentrations from 2uM to 10uM. Whereas, for similar concentrations, mutated GH25 (GH25mut) showed no significant increase in RFU/min compared to the active version. Commercial HEWL showed a steady increase in RFU/min from 1uM to 5.5uM concentrations (Figure 8C; Supplementary Figure S11C). Thus, the recombinant protein represents a functional GH25 hydrolase with a lysozyme activity.

To test for a direct function of the GH25 lysozyme, we treated *A. laibachii* -infected Arabidopsis plants with the recombinant protein. The impact of treatment of *A. laibachii* infection was quantified by quantitative PCR to determine the relative *A. laibachii* biomass on Arabidopsis in response to GH25. Strikingly, we observed a significant reduction of *A. laibachii* colonization in leaves treated with the active GH25 lysozyme, while the mutated enzyme GH25_D124E did not significantly influence infection (p-value of <0.0001 and an R-squared value of 98.88%**)** (Figure 8D)**.** Overall, treatment with the GH25 lysozyme reduced the amount of *A. laibachii* to about 50%.

Discussion

Healthy plants in natural habitats are extensively colonized by microbes, therefore it has been hypothesized that the immune system and the microbiota may instruct each other

beyond the simple co-evolutionary arms race between plants and pathogens (29). Community members as individuals or in a community context have been reported to confer extended immune functions to their plant host. Root endophytic bacteria for example were found to protect *A. thaliana* and stabilize the microbial community by competing with filamentous eukaryotes (30). A large inhibitory interaction network was found in the leaf microbiome of *A. thaliana* and genome mining was used to identify over 1000 predicted natural product biosynthetic gene clusters (BGCs) (31). In addition, the bacterium *Brevibacillus* sp. leaf 182 isolate was found to inhibit half of the 200 strains isolated from *A. thaliana* phyllosphere. Further analysis revealed that *Brevibacillus* sp. leaf 182 produces a trans-acyltransferase polyketide synthase-derived antibiotic, macrobrevin along with other putative polyketide synthases (31).

In this study, we describe the role of the basidiomycete yeast *MbA,* which we previously co-isolated with the oomycete pathogen *A. laibachii* and now characterized as an antagonistic driver in the *A. thaliana* phyllosphere. *A. laibachii* inhibits *in-vitro* growth of seven members of a bacterial leaf SynCom and, most strikingly, strongly suppresses disease progression and reproduction of the pathogenic oomycete *A. laibachii* on *A. thaliana*. *MbA* is a member of the Ustilaginales, which had previously been classified into the group of pathogenic smut fungi of the *Moesziomyces bullatus* species (11). Our genome analysis identified the anamorphic yeasts *M. rugulosus, M. aphidis* and *M. antarcticus*, which had previously been classified as "*Pseudozyma spec*.", as the closest relatives of *MbA*. Anamorphic Ustilaginales yeasts are long known and have been used for biotechnological applications and also biocontrol (32). Mannosylerythritol lipids produced by *M. antarcticus* are known to act as biosurfactants and are of great interest for pharmaceutical applications (33,34). Glycolipids like flocculosin produced by *A. flocculosa* or ustilagic acid characterized in the smut fungus *U. maydis*, have antifungal activity. Those compounds destabilize the membrane of different fungi and thus serve as biocontrol agents against powdery mildews or grey mold (35–37)

We identified 13 potential secondary metabolite gene clusters in *MbA,* including non-ribosomal peptide synthases and polyketide synthetase. Interaction among microbes within the same habitat is believed to have given rise to a variety of secondary metabolites (38,39). The presence of *Streptomyces rapamycinicus* was shown to

activate an otherwise silent polyketide synthase gene cluster, *fgnA*, in *Aspergillus fumigatus.* The resultant compound proved to be a potent fungal metabolite that inhibited the germination of *S. rapamycinicus* spores (40). Therefore, secondary metabolite gene clusters and their corresponding products may confer a competitive advantage to fungi over the bacteria that reside in the same environment.

What is still under debate is the relation of anamorphic yeasts with the related pathogenic smuts. Many smut fungi, including the model species *U. maydis* are dimorphic organisms. In their saprophytic phase they grow as haploid non-pathogenic yeast cells. Only on appropriate host surfaces, haploid cells switch to filamentous growth and expression of pathogenicity-related genes is only activated upon mating in the filamentous dikaryon. A prime prerequisite for pathogenic development is therefore the ability of mating (41,42). Our genome analysis identified a tetrapolar mating system with a complete set of mating genes in *MbA*. Looking more closely on the phylogeny of different mating genes it appears that all sequenced *Moesziomyces* strains have the same pheromone receptor type (Supplementary Figure S12). Together with our unsuccessful mating assays, this suggests that all sequenced strains of this species have the same mating type and, therefore, are unable to mate. Mating type bias after spore germination was reported for *Ustilago bromivora,* which leads to a haplo-lethal allele linked to the MAT-2 locus (43). In this case, an intratetrad mating event rescues pathogenicity in nature as the second mating partner is not viable after spore germination. Together with the observation that anamorphic *Moesziomyces* yeasts are ubiquitous in nature, one could hypothesize that these fungi are highly competitive in their haploid form and antagonism might have led to the selection of one viable mating type. This eventually adapted to the epiphytic life style.

Transcriptome analysis showed that epiphytic growth of *MbA* on *A. thaliana* leads to massive transcriptional changes particularly in primary metabolism, which might reflect adaptation to the nutritional situation on the plant surface. Moreover, *MbA* showed specific transcriptional responses to a bacterial community, as well as to *A. laibachii* when being co-inoculated on plant leaves. Presence of *A. laibachii* resulted in the induction of primary metabolism and biosynthesis pathways, which might reflect enhanced growth of *MbA* in the presence of *A. laibachii.*

A set of *MbA* genes encoding secreted hydrolases was induced by *A. laibachii* and one of these genes which encodes a putative GH25 hydrolase with similarity to *Chalaropsis* type lysozymes appeared to be essential for the biocontrol of *A. laibachii*. Initially discovered in the fungi *Chalaropsis* sp., this group of proteins is largely present in bacteria as well as phages for example the germination specific muramidase from *Clostridium perfringens* S40 (44). The bacterial muramidase, cellosyl from *Streptomyces coelicolor* (45) also belongs to the *Chalaropsis*type of lysozyme. These proteins are proposed to cleave the β-1,4-glycosidic bond between N-acetylmuramic acid (NAM) and N-acetylglucosamine (NAG) in the bacterial peptidoglycan. Specifically, the β -1,4-N,6-O-diacetylmuramidase activity allows the *Chalaropsis* type lysozyme to degrade the cell wall of *Staphylococcus aureus*, in contrast to the commercially available Hen egg-white lysozyme (HEWL) (45). Despite differences in structure and molecular weight from HEWL, the GH25 of MbA has lysozyme activity against the gram positive bacterium *Micrococcus lysodeikticus* in a fluorogenic assay. This highlights the overall biochemical functionality of the recombinant glycoside hydrolase. The glycoside Hydrolase 25 family is predicted to have an active site motif DXE which is highly conserved across the fungal kingdom (Supplementary Figure S13). The structure of glycoside hydrolase family 25 from *Aspergillus fumigates* was characterized and the presence of N-terminal signal peptide was considered to indicate an extracellular secretion of the protein with possible antimicrobial properties (46). The role of the secreted hydrolase in the fungal kingdom is not completely explored yet. The presence of such hydrolases has in many cases been hypothesized to be associated with hyperparasitism of fungi parasitizing fungi (47) or oomycetes parasitizing oomycetes (48). Our results might therefore indicate a cross kingdom hyperparasitism event between a fungus and an oomycete. Previous work on microbial communities has indicated that negative interactions stabilize microbial communities. Hyperparasitism is such a negative interaction with a strong eco-evolutionary effect on pathogen-host interactions and therefore on community stability (49). *MbA* might therefore regulate *A. laibachii* infection and reduce disease severity. The qPCR evaluation of oomycete biomass strongly points towards the idea that *A. laibachii* is a direct target of antagonism for MBA. Since we observed reduced formation of *A. laibachii* in presence

of *MbA*, we also tested if the GH25 lysozyme would suppress zoospore germination. However, we could not detect a significant reduction of *A. laibachii* zoosporangia germination upon treatment with active GH25 lysozyme (Supplementary figure S14), suggesting that the GH25 lysozyme interferes with *A. laibachii* at a later stage of infection. As *A. laibachii* has been shown to reduce microbial diversity (7), *MbA* might increase diversity through hyperparasitism of *A. laibachii*. At the same time this increased diversity might have caused the need for more secondary metabolites to evolve in the *MbA* genome to defend against niche competitors. Through its close association with *A. laibachii*, *MbA* could be a key regulator of the *A. thaliana* microbial diversity and therefore relevant for plant health beyond the regulation of *A. laibachii* infection.

In conclusion, the secreted hydrolase we identified as main factor of *A. laibachii* inhibition has great potential to act as antimicrobial agent. The isolated compound is not only valuable per se in an ecological context. It can further lay the grounds for exploring other microbial bioactive compounds that mediate inter-species and inter-kingdom crosstalk. A main goal of our future studies will be to understand on the mechanistic level, how the GH-25 suppresses *A. laibachii*, and at which developmental step the oomycete infection is blocked. Since the GH-25 enzyme is well conserved amongst Ustilaginales including pathogenic species, it will also be tempting to elucidate whether the species-specific antagonism identified here is broadly conserved among Ustilaginales fungi and oomycetes. We further will investigate potential responses by the host plant and how this impacts *A. laibachii* growth upon *MbA* colonization. Functional investigation of these interactions can provide meaningful insights as to why certain yeasts prefer to colonize specific environments. At the same time, it will be worth exploring how the basidiomycete yeasts influence the bacterial major colonizers of the phyllosphere.

Material and Methods

Strains and growth conditions

MbA wildtype strain was isolated from *A. laibachii* infected *A. thaliana* leaves [7]. Wild-type *MbA* (at 22 degrees) and *U. maydis* (at 28 degrees) strains were grown in liquid

YEPSlight medium and maintained on Potato dextrose agar plates. King's B medium was used for culturing Syn Com bacterial members at 22 degrees. All the strains were grown in a rotary shaker at 200rpm. All the recipes for medium and solutions can be found in Supplementary Table S2. Stress assays for fungi: wildtype and mutant strains of *MbA* grown to an optical density (600 nm) of 0.6-0.8 were centrifuged at 3500rpm for 10 minutes and suspended in sterile water to reach an OD of 1.0. Next, a dilution series from 10^0 to 10-4 was prepared in sterile H_2O. In the end, 5 µl of each dilution were spotted on CM plates supplemented with the indicated stress agents. The plates were incubated for 2 days at 22°C. Confrontation assays: at first, *MbA* and SynCom bacterial strains were grown to an O.D of 0.8-1. *MbA* cultures (10ul) were dropped in four quadrants of a Potato Dextrose Agar plate, previously spread with a bacterial culture. Plates were incubated for 2-4 days at 22°C.

Transformation of *MbA* and plasmid construction for generation of knockout mutants

Fungal strains were grown in YEPSL at 22°C in a rotary shaker at 200rpm until an O.D. of 0.6 was reached and centrifuged for 15 mins at 3500rpm. The cells were washed in 20 ml of SCS (Table S2), and further centrifuged for 10 minutes at 3000rpm, before being treated with 3ml SCS solution with 20mg/ml of Glucanex (Lysing Enzyme from *Trichoderma harzianum*, # L1412, Sigma). After 20 minutes of incubation at room temperature, as cell wall lysis was occurred, cold SCS was added to the mix and protoplasts spun down for 10 minutes at 2400rpm. They were then washed twice with SCS and resuspended with 10 ml STC (SupplementaryTable S2) to be centrifuged at 2000rpm for 10 minutes. Finally, the pellet was dissolved in 500 µl STC, and stored in aliquots of 50 µl at -80°C. 5µg of plasmid DNA along with 15 µg Heparin was added to 50 µl protoplasts. After incubation on ice for 10 minutes, STC/40%PEG (500 µl) was added to it and mixed gently by pipetting up and down; this step was followed by another 15 minutes on ice. The transformation mix was added to 10 ml of molten regeneration (reg) agar and poured over a layer of already solidified reg agar containing appropriate antibiotic solution. For the bottom layer, we used 400 µg/ml Hygromycin/ 8 µg/ml Carboxin/ 300 µg/ml nourseothricin (NAT).

Plasmids were cloned using *Escherichia coli* DH5α cells (Invitrogen, Karlsruhe, Germany). Construction of deletion mutants was performed by homologous recombination; the 5' and 3' flanking regions of the target genes were amplified and ligated to an antibiotic resistance cassette (50). The ligated fragment was subsequently transformed into *MbA*. Homologous integration of the target gene was verified via PCR on the antibiotic resistant colonies. Oligonucleotide pairs for knockout generation and verification can be found in Supplementary Table S3. PCR amplification was done using Phusion© DNA polymerase (Thermo Scientific, Bonn, Germany), following the manufacturer's instructions, with 100 ng of genomic DNA or cDNA as template. Nucleic acids were purified from 1% TAE agarose gels using Macherey-Nagel™ NucleoSpin™ Gel and PCR Clean-up Kit.

Mating assay and generation of the self-compatible *MbA* strain CB1

Haploid strains of *MbA* were grown in liquid cultures, mixed and drops arranged on PD-plates with charcoal to induce filament formation. Plate with the haploid *U. maydis* strains FB1 and FB2 and the solopathogenic strain SG200 served as internal control.

The complete b-locus of the solopathogenic *U. hordei* strain DS200 was amplified (Figure S2) and inserted into the *MbA* b-locus by homologous recombination. The strain obtained, known as compatible b1 (CB1) was tested positive by amplification of the right border and left border areas with primers specific for the genomic locus and for the plasmid region. Additionally, two primers specific for the *MbA bE*and *bW* genes were chosen to amplify parts of the native locus. To induce filament and appressoria formation in vitro we used a *Moesziomyces* YEPSL culture at OD_{600} 0.6-0.8. The cells were diluted to an OD_{600} of 0.2 in 2% YEPSL (for appressoria formation 100µM 16-hydroxyhexadecanoic acid (Sigma-Aldrich) or 1% ethanol was added) and sprayed the yeast like cells on parafilm which mimics the hydrophobic plant surface. After 18h incubation at 100% humidity the number of cells grown as filaments (or generating appressoria) was determined relative to the total number of total cells by using a light microscope.

546 **_Arabidopsis thaliana_ leaf infections and quantification of Albugo biomass**
547 **quantification by qPCR**

548 Sterilized *Arabidopsis thaliana* seeds were subjected to cold treatment for 7 days and
549 sown on 1/2 strength Murashige Skoog (MS) medium (Supplementary Table S2). The
550 MS plates are directly transferred to growth chambers having 22°C on a short-day
551 period (8 h light) with (33-40%) humidity and grown for 4 weeks before inoculation.
552 Overnight liquid cultures of *MbA* and SynCom bacterial strains were grown to an OD_{600}
553 of 0.6. The cultures were spun down at 3500rpm for 10 minutes and the pellets
554 dissolved in $MgCl_2$. 500µl of each culture was evenly sprayed on three-week old *A.*
555 *thaliana* seedlings using airbrush guns. Two days later, a spore solution of *A. laibachii*
556 was then sprayed on the seedlings following the protocol of Ruhe et al. (51). Two weeks
557 later, the disease symptoms on the leaves were scored as a percentage between
558 infected and non-infected leaves.
559 4 weeks old *A. thaliana* seedlings on MS plates were sprayed with *A. laibachii* as a
560 control and GH25+ *A.laibachii* and *Mut_GH25+A.laibachii* as treatments. After 10 days
561 post infection (dpi), the seedlings were harvested, frozen in liquid nitrogen and kept at -
562 80°C. For DNA extraction, the frozen plant material was ground into a fine powder with
563 mortar and pestle and treated with extraction buffer (50 mM Tris pH 8.0, 200 mM
564 NaCl,0.2 mM ethylenediaminetetraacetic acid (EDTA), 0.5% SDS,0.1 mg/ml proteinase
565 K (Sigma–Aldrich). This was followed centrifugation after the addition of one volume
566 Phenol/Chloroform/Isoamylalkohol 25:24:1 (Roth). The top aqueous layer was removed
567 and added to one volume of Isopropanol to precipitate the nucleic acids. DNA pellet
568 obtained after centrifugation was washed with 70% EtOH and finally dissolved in 50 ul
569 Nuclease-free water. For qPCR measurements; 10 ul of GoTaq® qPCR 2x Master Mix
570 was used (Promega, Waltham, Madison, USA); 5ul of DNA (~50ng); 1ul of forward and
571 reverse primer (10µM) up to a total volume 20µl. Samples were measured in triplicates
572 in a CFX Connect real-time PCR detection system (Bio-Rad) following protocol of Ruhe
573 et al. (2016)(51). Amount of *A. laibachii* DNA was quantified using the following
574 oligonucleotide sequences, (A. thalianaEF1-α: 5′-AAGGAGGCTGCTGAGATGAA-3′, 5′-
575 TGGTGGTCTCGAACTTCCAG-3′; Oomycete internal transcribed spacer (ITS) 5.8s: 5′-
576 ACTTTCAGCAGTGGATGTCTA-3′, 5′-GATGACTCACTGAATTCTGCA-3′). Cq values

obtained in case of the oomycete DNA amplification was normalized to *A. thalaina* DNA amplicon and then the difference between control (only *Albugo*) and treatment (*Albugo*+ GH25/Mut_GH25) was calculated by ddCq. The relative biomass of *Albugo* was analyzed by the formula (2^{-ddCq}). Each data point in the graph represent three independent biological replicates.

Nucleic acid methods

RNA-Extraction of Latex-peeled samples: Four weeks old *A. thaliana* plants were fixed between two fingers and liquid latex was applied to the leaf surface by using a small brush. The latex was dried using the cold air option of a hair dryer, carefully peeled off with a thin tweezer and immediately frozen in liquid nitrogen. Afterwards, the frozen latex pieces were grinded with liquid nitrogen and the RNA was isolated by using Trizol® Reagent (Invitrogen, Karlsruhe, Germany) according to the manufacturer's instructions. Turbo DNA-Free™ Kit (Ambion, life technologies™, Carlsbad, California, USA) was used to remove any DNA contamination in the extracted RNA. Synthesis of cDNA was performed using First Strand cDNA Synthesis Kit (Thermo Fischer scientific, Waltham, Massachusetts, USA) according to recommended instruction starting with a concentration of 10µg RNA. QIAprep Mini Plasmid Prep Kit (QIAGEN, Venlo, Netherlands) was used for isolation of plasmid DNA from bacteria after the principle of alkaline lysis. Genomic DNA was isolated using phenol-chloroform extraction protocol (18).

RT-qPCR oligonucleotide pairs were designed with Primer3 Plus. The oligonucleotide pairs were at first tested for efficiency using a dilution series of genomic DNA. The reaction was performed in a Bio-Rad iCycler system using the following conditions: 2 min at 95 °C, followed by 45 cycles of 30 s at 95 °C, 30 s at 61 °C and generation of melting curve between 65°C to 95°C.

Bioinformatics and computational data analysis

Sequence assembly of *MbA* strains was performed using the HGAP pipeline (Pacific Biosciences). *MbA* genome was annotated with the Augustus software tool. Secretome was investigated using SignalP4.0. Analysis of functional domains in the secreted

proteins was done by Inter-Pro Scan. AntiSmash was used to predict potential secondary metabolite clusters. RNA sequencing was done at the CCG- Cologne Center for Genomics by using a poly-A enrichment on an Illumina HiSeq4000 platform. The achieved paired end reads were mapped to the *MbA* and *A. thaliana* TAIR10 genome by using Tophat2 (28). RNA-Seq reads of *MbA* axenic cultures were used to generate exon and intron hints and to start a second annotation with Augustus. Heat-maps were performed using the heatmap.2 function of the package gplots (version 3.0.1) in r-studio (R version 3.5.1). An analysis of variance (ANOVA) model was used for pairwise comparison of the conditions, with Tukey's HSD test to determine significant differences among them (*P* values <0.05).

Heterologous protein production and GH25 activity assay

The *Pichia pastoris* KM71H-OCH gene expression system was used to produce MBA_GH25 domain tagged with an N-terminal Pilyhistidine tah (6XHis) and a C-terminal peptide containing the c-myc epitope and a 6xHis tag. The His-MspGH25 cloned into pGAPZαA vector (Invitrogen, Carlsbad, CA, USA) under the control of a constitutive promotor with an α-factor signal peptide for secretion. Expression and purification of recombinant proteins were performed according to manufacturer's instructions (Invitrogen Corporation, Catalog no. K1710-01): YPD medium supplemented with 100 µg ml^{-1} zeocin was used for initial growth of *P. pastoris* strains at 28°C and 200 rpm (for liquid cultures). Production of the recombinant protein was performed in 1 L buffered (100 mM Potassium phosphate buffer, pH 6.0) YPD medium with 2% Sucrose at 28°C for 24 hours with 200 rpm shaking. Next the protein was subjected to affinity purification with a Ni-NTA-matrix, according to manufacturer's instructions (Ni-Sepharose™ 6 Fast-Flow, GE-Healthcare; Freiburg, Germany). After purification, the His-MspGH25 protein was dialyzed in an exchange buffer (0.1M NaPi, 0.1M Nacl, pH=7.5). The purified protein was kept in 100 µl aliquots at 4°C.

Site directed mutagenesis was performed on pGAPZα-His- MspGH25 vector according to the instructions of the QuikChange Multi Site-Directed Mutagenesis Kit (Agilent Technologies, Santa Clara, United States) with primers targeting nucleotides of the active site of GH25.

Purified Glycoside Hydrolase of *MBA* from P. pastoris was quantified according to a sensitive fluorescence-based method using Molecular Probes™ EnzChek™ Lysozym-Assay-Kit (ThermoFisher Scientific, Katalognummer: E22013). DQ lysozyme substrate (*Micrococcus lysodeikticus*) stock suspension (1.0mg/ml) and 1000units/ml Hen egg White Lysozyme (HEWL) stock solution were prepared according to the manufacturer. Molar concentration of the HEWL stock solution was calculated using the following website (https://www.bioline.com/media/calculator/01_04.html) and was found to be 11µM. Protein concentration of MspGH25 (both active and mutated version was measured in the Nanodrop 2000c spectrophotometer (Thermo Fischer scientific, Waltham, Massachusetts, USA) according to manufacturer's instructions using 100 µl of sample after using 100 µl of the appropriate buffer as a blank control in glass cuvette. The molar concentrations of recombinant proteins were also calculated as above.

Starting the reaction 50µl of the DQ lysozyme substrate working suspension was added to each microplate well containing reaction buffer with either HEWL (in molar concentrations ranging from 0.1-5.5µM) or MspGH25 (in molar concentration from 0.5-17.5µM). Fluorescence intensity of each reaction was measured every 5min to follow the kinetic of the reaction at 37°C for 60min, using fluorescence microplate reader with fluorescein filter Tecan Infinite 200 Pro plate reader (Tecan Group Ltd., Männendorf, Switzerland). Digestion products from the DQ lysozyme substrate have an absorption maximum at ~494nm and a fluorescence emission maximum at ~518nm.

Data availability

Genome information and RNA sequencing have been submitted to NCBI Genbank and are available under the following links: https://www.ncbi.nlm.nih.gov/geo/query/acc.cgi?acc=GSE148670

Acknowledgments

This work was funded through by the Deutsche Forschungsgemeinschaft (DFG, German Research Foundation) under Germany's Excellence Strategy EXC-2048/1,

Project ID 390686111, and the DFG priority program SPP2125 “DECRyPT”. We are grateful to Marco Thines for generously providing *M. bullatus* wild type strains. We thank Libera Lo Presti for critically reading the manuscript and helpful comments and suggestion.

References

1. Ritpitakphong U, Falquet L, Vimoltust A, Berger A, Métraux JP, L’Haridon F. The microbiome of the leaf surface of Arabidopsis protects against a fungal pathogen. New Phytologist. 2016;

2. Walker TS, Bais HP, Grotewold E, Vivanco JM. Root exudation and rhizosphere biology. Plant Physiology. 2003;

3. Bulgarelli D, Schlaeppi K, Spaepen S, van Themaat EVL, Schulze-Lefert P. Structure and Functions of the Bacterial Microbiota of Plants. Annual Review of Plant Biology. 2013;

4. Busby PE, Peay KG, Newcombe G. Common foliar fungi of Populus trichocarpa modify Melampsora rust disease severity. New Phytologist. 2016;

5. Mikiciński A, Sobiczewski P, Puławska J, Maciorowski R. Control of fire blight (Erwinia amylovora) by a novel strain 49M of Pseudomonas graminis from the phyllosphere of apple (Malus spp.). European Journal of Plant Pathology. 2016;

6. Stone BWG, Weingarten EA, Jackson CR. The Role of the Phyllosphere Microbiome in Plant Health and Function. In: Annual Plant Reviews online. 2018.

7. Agler MT, Ruhe J, Kroll S, Morhenn C, Kim ST, Weigel D, et al. Microbial Hub Taxa Link Host and Abiotic Factors to Plant Microbiome Variation. PLoS Biology. 2016;

8. Coyte KZ, Schluter J, Foster KR. The ecology of the mCoyte, K.Z., Schluter, J. & Foster, K.R. (2015) The ecology of the microbiome: Networks, competition, and stability. Science, 350, 663–666.icrobiome: Networks, competition, and stability. Science. 2015;

9. Vorholt JA. Microbial life in the phyllosphere. Nature Reviews Microbiology. 2012;

10. Brefort T, Doehlemann G, Mendoza-Mendoza A, Reissmann S, Djamei A, Kahmann R. Ustilago maydis as a Pathogen. Annual Review of Phytopathology. 2009;

11. Kruse J, Doehlemann G, Kemen E, Thines M. Asexual and sexual morphs of Moesziomyces revisited. IMA Fungus. 2017;

12. Wang QM, Begerow D, Groenewald M, Liu XZ, Theelen B, Bai FY, et al. Multigene phylogeny and taxonomic revision of yeasts and related fungi in the Ustilaginomycotina. Studies in Mycology. 2015;81:55–83.

13. Barda O, Shalev O, Alster S, Buxdorf K, Gafni A, Levy M. Pseudozyma aphidis induces salicylic-acid-independent resistance to Clavibacter michiganensis in tomato plants. Plant Disease. 2015;

14. Gafni A, Calderon CE, Harris R, Buxdorf K, Dafa-Berger A, Zeilinger-Reichert E, et al. Biological control of the cucurbit powdery mildew pathogen Podosphaera xanthii by means of the epiphytic fungus Pseudozyma aphidis and parasitism as a mode of action. Frontiers in Plant Science. 2015;

15. Lee G, Lee SH, Kim KM, Ryu CM. Foliar application of the leaf-colonizing yeast Pseudozyma churashimaensis elicits systemic defense of pepper against bacterial and viral pathogens. Scientific Reports. 2017;

16. Zuo W, Ökmen B, Depotter JRL, Ebert MK, Redkar A, Misas Villamil J, et al. Molecular Interactions Between Smut Fungi and Their Host Plants. Annual Review of Phytopathology. 2019;

17. Stanke M, Steinkamp R, Waack S, Morgenstern B. AUGUSTUS: A web server for gene finding in eukaryotes. Nucleic Acids Research. 2004;

18. Kämper J, Kahmann R, Bölker M, Ma LJ, Brefort T, Saville BJ, et al. Insights from the genome of the biotrophic fungal plant pathogen Ustilago maydis. Nature. 2006;

19. Redkar A, Hoser R, Schilling L, Zechmann B, Krzymowska M, Walbot V, et al. A secreted effector protein of Ustilago maydis guides maize leaf cells to form tumors. Plant Cell. 2015;

20. Schirawski J, Mannhaupt G, Münch K, Brefort T, Schipper K, Doehlemann G, et al. Pathogenicity determinants in smut fungi revealed by genome comparison. Science. 2010;

21. Bölker M, Urban M, Kahmann R. The a mating type locus of U. maydis specifies cell signaling components. Cell. 1992;

22. Lefebvre F, Joly DL, Labbé C, Teichmann B, Linning R, Belzile F, et al. The transition from a phytopathogenic smut ancestor to an anamorphic biocontrol agent deciphered by comparative whole-genome analysis. Plant Cell. 2013;

23. Sharma R, Ökmen B, Doehlemann G, Thines M. Saprotrophic yeasts formerly classified as Pseudozyma have retained a large effector arsenal, including functional Pep1 orthologs. Mycological Progress. 2019;

24. Brefort T, Tanaka S, Neidig N, Doehlemann G, Vincon V, Kahmann R. Characterization of the Largest Effector Gene Cluster of Ustilago maydis. PLoS Pathogens. 2014;

25. Dutheil JY, Mannhaupt G, Schweizer G, Sieber CMK, Münsterkötter M, Güldener U, et al. A tale of genome compartmentalization: The evolution of virulence clusters in smut fungi. Genome Biology and Evolution. 2016;

26. Khrunyk Y, Münch K, Schipper K, Lupas AN, Kahmann R. The use of FLP-mediated recombination for the functional analysis of an effector gene family in the biotrophic smut fungus Ustilago maydis. New Phytologist. 2010;

27. Mendoza-Mendoza A, Berndt P, Djamei A, Weise C, Linne U, Marahiel M, et al. Physical-chemical plant-derived signals induce differentiation in Ustilago maydis. Molecular Microbiology. 2009;

28. Kim D, Pertea G, Trapnell C, Pimentel H, Kelley R, Salzberg SL. TopHat2: Accurate alignment of transcriptomes in the presence of insertions, deletions and gene fusions. Genome Biology. 2013;

29. Vannier N, Agler M, Hacquard S. Microbiota-mediated disease resistance in plants. PLoS Pathogens. 2019;

30. Durán P, Thiergart T, Garrido-Oter R, Agler M, Kemen E, Schulze-Lefert P, et al. Microbial Interkingdom Interactions in Roots Promote Arabidopsis Survival. Cell. 2018;

31. Helfrich EJN, Vogel CM, Ueoka R, Schäfer M, Ryffel F, Müller DB, et al. Bipartite interactions, antibiotic production and biosynthetic potential of the Arabidopsis leaf microbiome. Nature Microbiology. 2018;

32. Boekhout T. Pseudozyma Bandoni emend: Boekhout (1985) and a comparison with the yeast state of Ustilago maydis (De Candolle) Corda (1842). In: The Yeasts. 2011.

33. Kitamoto D, Akiba S, Hioki C, Tabuchi T. Extracellular accumulation of mannosylerythritol lipids by a strain of candida antarctica. Agricultural and Biological Chemistry. 1990;

34. Morita T, Konishi M, Fukuoka T, Imura T, Kitamoto D. Microbial conversion of glycerol into glycolipid biosurfactants, mannosylerythritol lipids, by a basidiomycete yeast, Pseudozyma antarctica JCM 10317T. Journal of Bioscience and Bioengineering. 2007;

35. Cheng Y, McNally DJ, Labbé C, Voyer N, Belzile F, Bélanger RR. Insertional mutagenesis of a fungal biocontrol agent led to discovery of a rare cellobiose lipid with antifungal activity. Applied and Environmental Microbiology. 2003;

774 36. Mimee B, Labbé C, Pelletier R, Bélanger RR. Antifungal activity of flocculosin, a
775 novel glycolipid isolated from Pseudozyma flocculosa. Antimicrobial Agents and
776 Chemotherapy. 2005;

777 37. Teichmann B, Linne U, Hewald S, Marahiel MA, Bölker M. A biosynthetic gene
778 cluster for a secreted cellobiose lipid with antifungal activity from Ustilago maydis.
779 Molecular Microbiology. 2007;

780 38. Schroeckh V, Scherlach K, Nützmann HW, Shelest E, Schmidt-Heck W,
781 Schuemann J, et al. Intimate bacterial-fungal interaction triggers biosynthesis of
782 archetypal polyketides in Aspergillus nidulans. Proceedings of the National
783 Academy of Sciences of the United States of America. 2009;

784 39. Rutledge PJ, Challis GL. Discovery of microbial natural products by activation of
785 silent biosynthetic gene clusters. Nature Reviews Microbiology. 2015;

786 40. Stroe MC, Netzker T, Scherlach K, Krüger T, Hertweck C, Valiante V, et al.
787 Targeted induction of a silent fungal gene cluster encoding the bacteria-specific
788 germination inhibitor fumigermin. eLife. 2020;

789 41. Bölker M. Ustilago maydis - A valuable model system for the study of fungal
790 dimorphism and virulence. Microbiology. 2001;

791 42. Nadal M, Gold SE. The autophagy genes atg8 and atg1 affect morphogenesis and
792 pathogenicity in Ustilago maydis. Molecular Plant Pathology. 2010;

793 43. Rabe F, Bosch J, Stirnberg A, Guse T, Bauer L, Seitner D, et al. A complete toolset
794 for the study of Ustilago bromivora and Brachypodium sp. as a fungal-temperate
795 grass pathosystem. eLife. 2016;

796 44. Chen Y, Miyata S, Makino S, Moriyama R. Molecular characterization of a
797 germination-specific muramidase from Clostridium perfringens S40 spores and
798 nucleotide sequence of the corresponding gene. Journal of Bacteriology. 1997;

799 45. Rau A, Hogg T, Marquardt R, Hilgenfeld R. A new lysozyme fold. Crystal structure
800 of the muramidase from Streptomyces coelicolor at 1.65 Å resolution. Journal of
801 Biological Chemistry. 2001;

802 46. Korczynska JE, Danielsen S, Schagerlöf U, Turkenburg JP, Davies GJ, Wilson KS,
803 et al. The structure of a family GH25 lysozyme from Aspergillus fumigatus. Acta
804 Crystallographica Section F: Structural Biology and Crystallization
805 Communications. 2010;

806 47. Hyde KD, Xu J, Rapior S, Jeewon R, Lumyong S, Niego AGT, et al. The amazing
807 potential of fungi: 50 ways we can exploit fungi industrially. Fungal Diversity. 2019;

808 48. Horner NR, Grenville-Briggs LJ, van West P. The oomycete Pythium oligandrum
809 expresses putative effectors during mycoparasitism of Phytophthora infestans and
810 is amenable to transformation. Fungal Biology. 2012;

811 49. Parratt SR, Laine AL. The role of hyperparasitism in microbial pathogen ecology
812 and evolution. ISME Journal. 2016;

813 50. Kämper J. A PCR-based system for highly efficient generation of gene replacement
814 mutants in Ustilago maydis. Molecular Genetics and Genomics. 2004;

815 51. Ruhe J, Agler MT, Placzek A, Kramer K, Finkemeier I, Kemen EM. Obligate
816 biotroph pathogens of the genus albugo are better adapted to active host defense
817 compared to niche competitors. Frontiers in Plant Science. 2016;

818 52. Hemetsberger C, Mueller AN, Matei A, Herrberger C, Hensel G, Kumlehn J, et al.
819 The fungal core effector Pep1 is conserved across smuts of dicots and monocots.
820 New Phytologist. 2015;206(3):1116–1126.

821 53. Doehlemann G, Van Der Linde K, Aßmann D, Schwammbach D, Hof A, Mohanty
822 A, et al. Pep1, a secreted effector protein of Ustilago maydis, is required for
823 successful invasion of plant cells. PLoS Pathogens. 2009;

824 54. Schilling L, Matei A, Redkar A, Walbot V, Doehlemann G. Virulence of the maize
825 smut Ustilago maydis is shaped by organ-specific effectors. Molecular Plant
826 Pathology. 2014;

827 55. Seitner D, Uhse S, Gallei M, Djamei A. The core effector Cce1 is required for early
828 infection of maize by Ustilago maydis. Molecular Plant Pathology. 2018;

829 56. Krombach S, Reissmann S, Kreibich S, Bochen F, Kahmann R. Virulence function
830 of the Ustilago maydis sterol carrier protein 2. New Phytologist. 2018;

831 57. Schipper K. Charakterisierung eines Ustilago maydis Genclusters, das f€ur drei
832 neuartige sekretierte Effektoren kodiert. PhDitle. PhD thesis. 2009;

833 58. Doehlemann G, Reissmann S, Aßmann D, Fleckenstein M, Kahmann R. Two
834 linked genes encoding a secreted effector and a membrane protein are essential
835 for Ustilago maydis-induced tumour formation. Molecular Microbiology. 2011;

836 59. Ma LS, Wang L, Trippel C, Mendoza-Mendoza A, Ullmann S, Moretti M, et al. The
837 Ustilago maydis repetitive effector Rsp3 blocks the antifungal activity of mannose-
838 binding maize proteins. Nature Communications. 2018;

839 60. Djamei A, Schipper K, Rabe F, Ghosh A, Vincon V, Kahnt J, et al. Metabolic
840 priming by a secreted fungal effector. Nature. 2011;

841 61. Ökmen B, Kemmerich B, Hilbig D, Wemhöner R, Aschenbroich J, Perrar A, et al.
842 Dual function of a secreted fungalysin metalloprotease in Ustilago maydis. New
843 Phytologist. 2018;

844

845

846

847

848

Supporting information captions

Figure S1: Biocontrol activity of *MbA,* but not *U. maydis,* against bacterial SynCom members (7). Inhibition by *Moesziomyces* can be seen as a characteristic halo after 48hrs of co-incubation.

Figure S2: Trypan blue staining of *A. thaliana* leaves 15 days post infection with *A. laibachii*. (i) & (ii)- control set with only *A.laibachii* (error bar 50µm) ; (i)- Thick hyphal growth of *A.laibachii* on the leaf surface, (ii) appressoria formation can be seen (red arrow). (iii) & (iv) Treatment set (*MbA* sprayed two days before *Albugo* (iii): Zoospores aggregated together, with few of them forming hyphae (green box); in addition, short, broken hyphae visualized in some regions (red box), which have not been found in Control sets; (error bar- 200µm) (iv): A closer look at the broken hyphae, yellow arrow indicates germinating cysts of *A. laibachii* (error bar - 50µm)

Figure S3: Genome comparison of *MbA* and *Moesziomyces antarctica* T-34. Highlighted regions show that contigs with chromosomal rearrangements in MBA can be also found in the genome of the related species *Moesziomyces antarctica* T-34.

Figure S4: (A) Predicted secondary metabolite clusters in the genome of *MbA*. Most clusters have unpredictable functions, three belong to the type of terpene or nonribosomal peptide synthetase types and one is a polyketide synthetase cluster type I. (B) The gene cluster encoding for production of ustilagic acid,a well-studied secondary metabolite of smut fungi (37), is not present in the genome of *MbA*. (C) Out of the 13 predicted secondary metabolite clusters, three are unique to *MbA*. Cluster 2 is predicted to encode a terpene, cluster 8 is a cluster of unknown function and cluster 10 is predicted as NRPS cluster. Core biosynthetic genes are highlighted in red, additional biosynthetic genes in yellow and transport-related genes in blue, based on AntiSMASH predictions.

879 **Figure S5**: Protein alignment of the core effector Pep1 (52) from different
880 Ustilaginomycetes. (A) Pep1 regions important for functionality are present in all the
881 aligned sequences. Deletion of the *pep1* gene (UMAG_01987) in *U. maydis* leads to
882 complete loss of virulence, which can be restored by complementing the deletion
883 mutant with the *MbA pep1* gene (Ma1682). Infection of maize leaves was done as
884 described in (19). Disease symptoms were scored at 12 days post infection in three
885 independent biological replicates. n= number of plants infected
886
887 **Figure S6**: Comparison of known virulence clusters (18) between *U. maydis* and *MbA*.
888 Numbers are gene numbers (*UMAG_NUMBER* for *U. maydis*; *gNUMBER* for *MbA).*
889
890 **Figure S7:** Mating assays of *MbA* and different *M. bullatus* isolates. Mixing of haploid *U.*
891 *maydis* strains FB1 & FB2 and the solopathogenic strain SG200 served as a positive
892 control for mating on charcoal plates, wherein filamentous growth is indicated by white,
893 fluffy appearance of colonies. Haploid wild type strains without mating partner don't
894 show a fluffy phenotype. For all combinations of *Moesziomyces* strains, no mating event
895 resulting in filamentous growth on charcoal plates was observed.
896
897 **Figure S8**: A) Multi-dimensional scaling plot (MDS) plot based on the interactions of
898 *Moesziomyces* sp. (M.sp.) / *MbA* in response to the SynCom bacteria and
899 *Albugo laibachii* in three biological replicates. The MDS plot shows *Albugo* and non-
900 *Albugo* samples grouping together based on gene-level logCPM. (B) Voom mean-
901 variance trend of the dataset where points represent genes, and (C) sample-specific
902 weights obtained from the *limma-voom* function. Colours represent three replicates for
903 each treatment. Light blue: *MbA* on plant; Dark blue: *MbA* on plant + SynCom; Light
904 green: *MbA* on plant + Albugo; Dark green: *MbA* on plant + Albugo + SynCom.
905
906 **Figure S9**: (A) Sequence distribution of Gene Ontology terms. 60% of all the genes that
907 are downregulated in *MbA* on plant compared to axenic culture growth can be assigned
908 to GO-terms related to metabolism and cell cycle. (B) In contrast, presence of *A.*
909 *laibachii* leads to transcriptional activation of metabolic processes. 52% of all GO-terms

associated with genes upregulated in presence of *A. laibachii* are related to metabolic processes.

Figure S10: Stress assay of *MbA* wild type and knockout mutants of gene (g5, g5755 and g2490) respectively, on CM medium and 2% Glucose (A) with different conditions (B: 100 µg/ml Calcofluor; C: 150 µg/ml Calcoflour; D: 1 mMH2O2; E:45 µg/ml Congo-red; F: 1 M NaCl; G: 1 M Sorbitol). The strains were dropped on the CM plates containing different stress supplements in a dilution series from 10^0 to 10^{-4}

Figure S11: A) Recombinant MbA_GH25 was produced and purified using the *Pichia pastoris* protein expression system. The purified protein was loaded in a 12% SDS gel for visualization of an expected molecular weight of 27kDa for His-Tagged GH25. B) Schematic diagram of the recombinant construct, where the GH25 domain from MBA is tagged with an N-terminal polyhistidine Tag and a C-terminal peptide containing the c-myc epitope and a polyhistidine tag. C) Detection of lysozyme activity for Commercial Hen-egg white lysozyme (stock solution, 11µM) using the EnzChek[1] Lysozyme Assay Kit. The fluorescence was recorded every minute in a fluorescence microplate reader using excitation/emission of 485/530 nm in increasing concentrations from 0.1µM to 5.5 µM. Finally, Relative Fluorescence Unit (RFU)/ min was calculated for each concentration and plotted on the graph.

Figure S12: A molecular phylogenetic analysis using maximum likelihood estimation and based on pheromone receptor protein sequences similarity. *MbA* protein sequence clusters together with type 1 pheromone receptors of other Ustilaginomycetes.

Figure S13: Amino acid alignment of GH25 sequences from different fungi (see attached list –'GH25 with accession number', for full length sequences). The protein sequences were obtained from the NCBI database. Alignment was achieved using the PRALINE multiple sequence alignment program with default parameters. The scoring scheme works from 0 for the least conserved alignment position, up to 10 (indicated by *) for the most conserved alignment position. A conserved active-site DxE motif has

been predicted for glycoside hydrolase family 25. Sequences tested from different basiodiomycete, ascomycete and Chytrids, have the active site residue conserved (purple box).

Figure S14: Boxplot-analysis of GH 25 treatment on *in vitro A. laibachii* zoosporangial germination in three biological replicates analyzing about 100 zoosporangial cells for each replicate. A p value of 0.3 was obtained for paired T-test using one-tailed distribution.

Table S1: Composition of the bacterial SynCom

Table S2: *MbA* gene expression data

Table S3: Growth media and buffers used in this study

Table S4: PCR primers used in this study

Figure Legends

Figure 1: Position of *MbA* in the family of Ustilaginaceae. (A) molecular phylogenetic analysis by maximum likelihood method based on fungal ITS sequences and showing grouping of *MbA* with the millet pathogen *M. bullatus*. Pathogenic filamentous smuts (green) and anamorphic smut yeasts can be found across the phylogenetic tree. (B) Comparison of the morphology of *MbA* (bottom) and *U. maydis* (top) haploid cells grown in YEPSl$_{ight}$ medium to OD$_{600}$0.6.

Figure 2: Infection assay of *A. laibachii* on *A. thaliana*. Addition of a bacterial SynCom reduces the infection symptoms of *A. laibachii* at 14dpi. Those symptoms can be almost abolished by spraying *MbA* to the plant, independently of the presence of the bacterial community. Infections were performed in six individual replicates with 12 technical replicates. N indicates the number of infected plants that were scored for symptoms. An analysis of variance (ANOVA) model was used for pairwise comparison of the conditions, with Tukey's HSD test to determine differences among them. Different letters indicate significant differences (P values < 0.05).

Figure 3: Circos comparison of *MbA* and *U. maydis* chromosome structure (A). We highlighted potential secondary metabolite clusters, secreted proteins and gene predictions on both strands (+/-). (B) Homology based comparisons identified three chromosomal recombination events, which affects the *MbA* contigs 2, 6 & 8.

Figure 4: Structure of the largest virulence cluster (Cluster 19A) in pathogenic smut fungi and anamorphic smut yeasts (marked with*). Colors indicate genes with homology to each other: Related gene families are indicated in orange, yellow, blue, green and brown, whereas unique effector genes are shown in grey. Genes encoding proteins without a secretion signal are shown in white (24).

Figure 5: Genetic transformation of *MbA.* (A) Stable transformants that express cytosolic GFP could be obtained by generating protoplasts with Glucanex and ectopically integrating linear DNA-fragments into the genome via PEG-mediated transformation. (B) Overview of the split-marker approach that was used to generate deletion mutants via homologous recombination.

Figure 6: The self-compatible *MbA* strain CB1 (A) *MbA* mating type genes, unlike the ones of *U. hordei*, can be found on two different chromosomes similar to the tetrapolar mating type system of *U. maydis*. (B) To generate a self-compatible strain (CB1), the b-mating genes of *U.hordei* were integrated at the native *MbA b*-locus. (C) Unlike the *MbA* wild type strain (top left), strain CB1 (bottom left) shows a fluffy phenotype on charcoal plates and filamentous growth. *U. maydis* haploid F1 strain (top right) and self-compatible SG200 strain (bottom right) were used as negative and positive control, respectively. (D,E) Induction of filamentation and appressoria formation in strain CB1 was studied in three independent experiments. For this around 1000 cells for filament formation and around 600 cells for appressoria formation were analyzed and error bars indicate standard error. After incubation on a hydrophobic surface, both, filament and appressoria formation in strain CB1, were significantly different (* Chi-Square Test for Independence – $\alpha = 0{,}0001$) when compared to *MbA* wild type and similar to the level of

the self-compatible *U. maydis* strain SG00. *U. maydis* haploid F2 strain was used as negative control (18). Scale bar: 20µm. 16-HDD: 16-Hydroxyhexadecanoic acid.

Figure 7: Transcriptome analysis of *MbA* (A) Experimental setup used for the transcriptomic (RNA-Sequencing) analysis in *MbA*. (B) Venn diagrams showing differential regulated *MbA* genes after spraying of haploid cells onto the *A. thaliana* leaf surface. A total number of 801 genes were upregulated in response to *A. laibachii* in presence and absence of bacterial SynCom. 216 of the 801 genes were upregulated in both conditions. (C) Hierarchical clustering of the 27 *A. laibachii* - induced *MbA* genes that are predicted to encode secreted proteins. Of these genes, nine were selected as candidate microbe-microbe effector genes, based on their transcriptional upregulation and prediction to encode for extracellularly localized proteins.

Figure 8: A reverse-genetic approach to identify the *MbA* gene which is responsible for the suppression of *A. laibachii* infection. (A) Three candidate microbe-microbe effector genes (*g5*, *g5755* &*g2490*) were deleted in *MbA* and deletion strains were individually inoculated on *A. thaliana* together with *A. laibachii*. Inoculation of two independent *g2490 null* strains *(Δg2490_1; Δg2490_2)* resulted in significant and almost complete loss the biocontrol activity of *MbA*. While deletion of g5 resulted in a marginal reduction of disease symptoms at 14 days post infection, deletion of g5755 had no effect on *A. laibachii.* (B) Genetic complementation of the *g2490* deletion restores the biocontrol activity to wild type levels. Infections in (A) were performed in six, in (B) in three individual replicates. In each replicate 12 plants were infected. N indicates the number of infected plants that were scored for symptoms. Different letters indicate significant differences (P values < 0.05; ANOVA model for pairwise comparison with Tukey's HSD test). (C) Detection of lysozyme. Increasing concentrations of purified MbA_GH25 and MbA_GH25(D124E) were incubated with the DQ lysozyme substrate for an hour at 37 ˚C. The fluorescence was recorded every minute in a fluorescence microplate reader using excitation/emission of 485/530 nm. Finally, Relative Fluorescence Unit (RFU)/ min was calculated for each concentration and plotted on the graph. Each data point represents three technical replicates and three independent biological replicates as

indicated by the Standard Error Measurement (SEM) bars. An unpaired t-test was performed for the active GH25 and Mutant_GH25 sets giving the p-value of <0.0001; and R squared value of 77.24%. (D) Relative quantification of *A. laibachii* biomass in response to MbA_GH25 (active and mutant) treatment via qPCR. The Oomycete internal transcribed spacer (ITS) 5.8s, was normalized to *A. thaliana* EF1-α gene to quantify the amount of *A. laibachii* DNA in the samples, ten days post infection. Then relative biomass was calculated comparing control sets (Only Albugo) with *A. laibachii* treated with GH25 and *A. laibachii* treated with Mutant_GH25 by ddCT method. Unpaired t-test between GH25 and Mutant_GH25 sets gave a p-value of <0.0001 and an R-squared value of 98.88%.

Tables

Table 1: Comparison of Genomes and genomic features of known pathogenic and anamorphic Ustilaginomycetes.

	MbA	*U. bromivora*	*S. scitamineum*	*S. reilianum*	*U. maydis*	*U. hordei*	*M. pennsylvanicum*	*A. flocculosa*
Assembly statistics								
Total contig length (Mb)	18.3		19.5	18.2	19.7	20.7	19.2	23.2
Total scaffold length (Mb)		20.5	19.6	18.4	19.8	21.15	19.2	23.3
Average base coverage	50x	154x	30x	20x	10x	25x	339x	28x
N50 contig (kb)	705.1		37.6	50.3	127.4	48.7	43.4	38.6
N50 scaffold length (kb)		877	759.2	738.5	817.8	307.7	121.7	919.9
Chromosomes	21	23		23	23	23		
GC-content (%)	60.9	52.4	54.4	59.7	54	52	50.9	65.1
Coding (%)	62.8	54.4	57.8	62.6	56.3	54.3	54	66.3
Coding Sequence								
Percentage CDS (%)	69.5	59.8	62	65.9	61.1	57.5	56.6	54.3
Average gene size (bp)	1935	1699	1819	1858	1836	1708	1734	2097
Average gene density (gene/kb)	0.36	0.35	0.34	0.37	0.34	0.34	0.33	0.30
Protein-coding genes	6653	7233	6693	6648	6786	7113	6279	6877
Exons	11645	11154	10214	9776	9783	10907	9278	19318
Average exon size (bp)	1091	1101	1191	1221	1230	1107	527	658
Exons/gene	1.75	1.5	1.5	1.47	1.44	1.53	1.48	2.8
tRNA genes	150	133	116	96	111	110	126	176
Noncoding sequence								
Introns	9333	3921	3521	3103	2997	3161	2999	12427
Introns/gene	1.40	0.54	0.53	0.47	0.44	0.44	0.48	1.81
Average intron length	163	163	130.1	144	142	141	191.4	141

(base)								
Average intergenic distance (bp)	769	1054	1114	929	1127	1186	1328	1273
Secretome								
Protein with signal peptide	559		622	632	625	538	419	622
Secreted without TMD	380				467			737
- with known domain	260				264			554

[24,42]

Table 2: *MbA* proteins homologous to *U. maydis* effector genes with known virulence function.

Name	Homologue	Query cover	E-value	Identity (%)	*U. maydis* knockout phenotype	Reference
g1653	UMAG_01987 (Pep1)	82%	3-e56	60.96	complete loss of tumor formation - blocked in early stages of infection	(53)
g1828	UMAG_01829 (Afu1)	99%	0.0	71.57	organ specific effector - reduced virulence in seedling leaves	(54)
g2626	UMAG_12197 (Cce1)	98%	1e-48	60.16	complete loss of tumor formation - blocked in early stages of infection	(55)
g2765	UMAG_11938 (Scp2)	100%	1e-73	93.44	Reduced in virulence	(56)
g2910	UMAG_02475 (Stp1)	32%	3e-42	60.71	complete loss of tumor formation - blocked in early stages of infection	(57)
g3652	UMAG_02239 (See1)	43%	9e-11	54.90	organ specific effector - reduced virulence in seedling leaves	(19)
g3113	UMAG_01375 (Pit2)	*	*	*	complete loss of tumor formation - blocked in early stages of infection	(58)
g3279	UMAG_03274 (Rsp3)	10%	5e-20	70.11	strong attenuation of virulence – reduced tumor size and number	(59)
g5296	UMAG_05731 (Cmu1)	98%	3e-70	43.84	Reducedvirulence	(60)
g6183	UMAG_06098 (Fly1)	100%	0.0	81.85	Reducedvirulence	(61)
g5835	UMAG_05302 (Tin2)	87%	8e-24	37.81	Minor impact on tumor formation – reduced anthocyanin biosynthesis	(24)

Figure 1

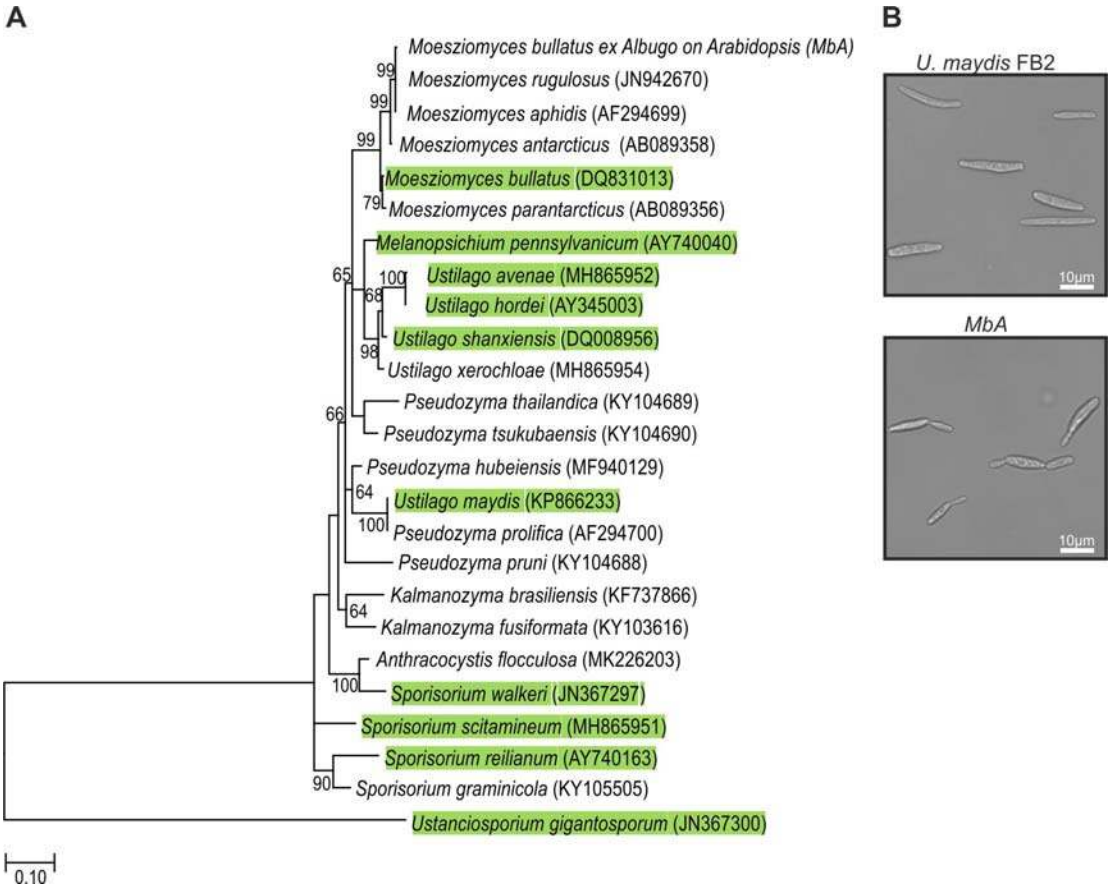

Figure 1: Position of *MbA* in the family of Ustilaginaceae. (A) molecular phylogenetic analysis by maximum likelihood method based on fungal ITS sequences and showing grouping of *MbA* with the millet pathogen *M. bullatus*. Pathogenic filamentous smuts (green) and anamorphic smut yeasts can be found across the phylogenetic tree. (B) Comparison of the morphology of *MbA* (bottom) and *U. maydis* (top) haploid cells grown in YEPSl$_{ight}$ medium to OD$_{600}$0.6.

Figure 2

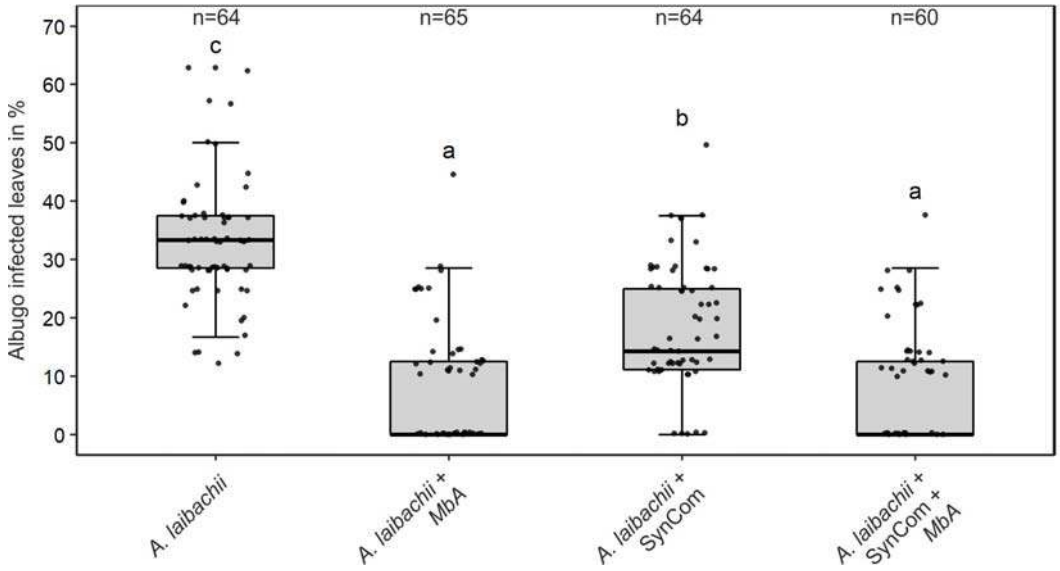

Figure 2: Infection assay of *A. laibachii* on *A. thaliana*. Addition of a bacterial SynCom reduces the infection symptoms of *A. laibachii* at 14dpi. Those symptoms can be almost abolished by spraying *MbA* to the plant, independently of the presence of the bacterial community. Infections were performed in six individual replicates with 12 technical replicates. N indicates the number of infected plants that were scored for symptoms. An analysis of variance (ANOVA) model was used for pairwise comparison of the conditions, with Tukey's HSD test to determine differences among them. Different letters indicate significant differences (P values < 0.05).

Figure 3

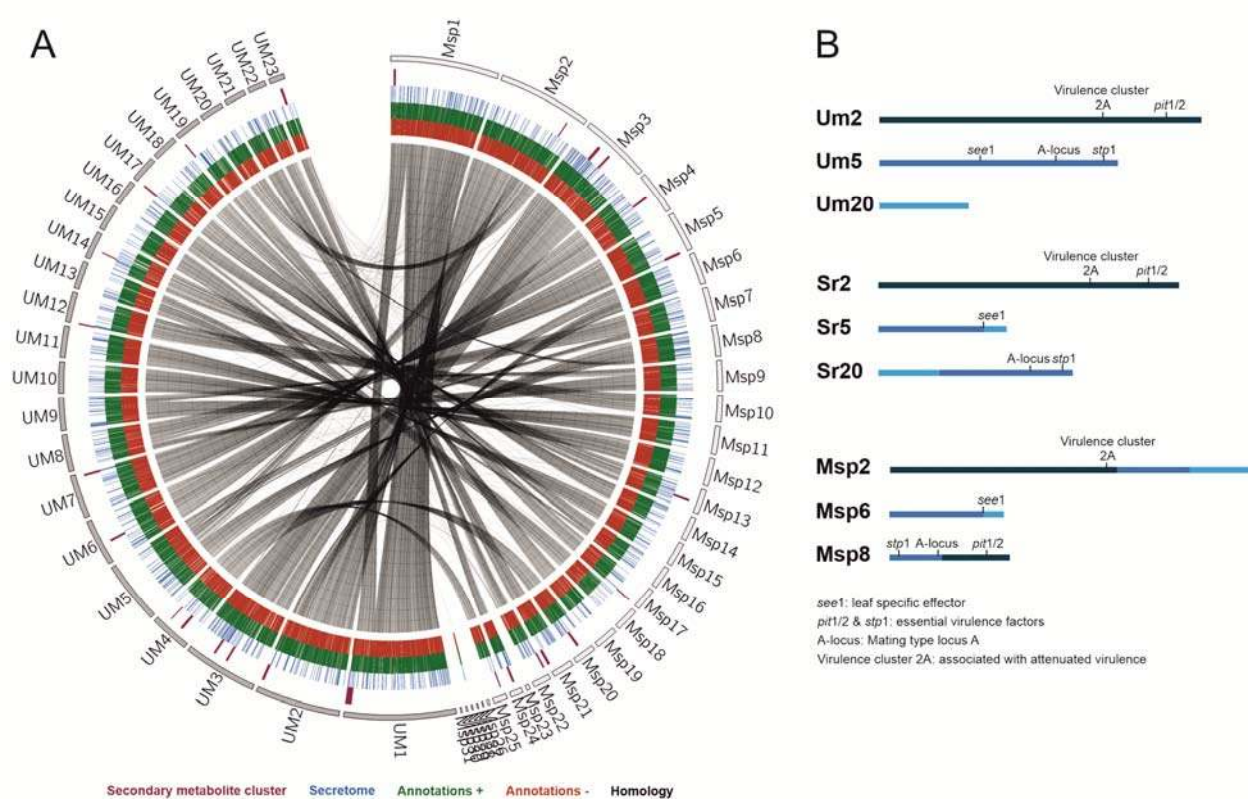

Figure 3: Circos comparison of *MbA* and *U. maydis* chromosome structure (A). We highlighted potential secondary metabolite clusters, secreted proteins and gene predictions on both strands (+/-). (B) Homology based comparisons identified three chromosomal recombination events, which affects the *MbA* contigs 2, 6 & 8.

Figure 4

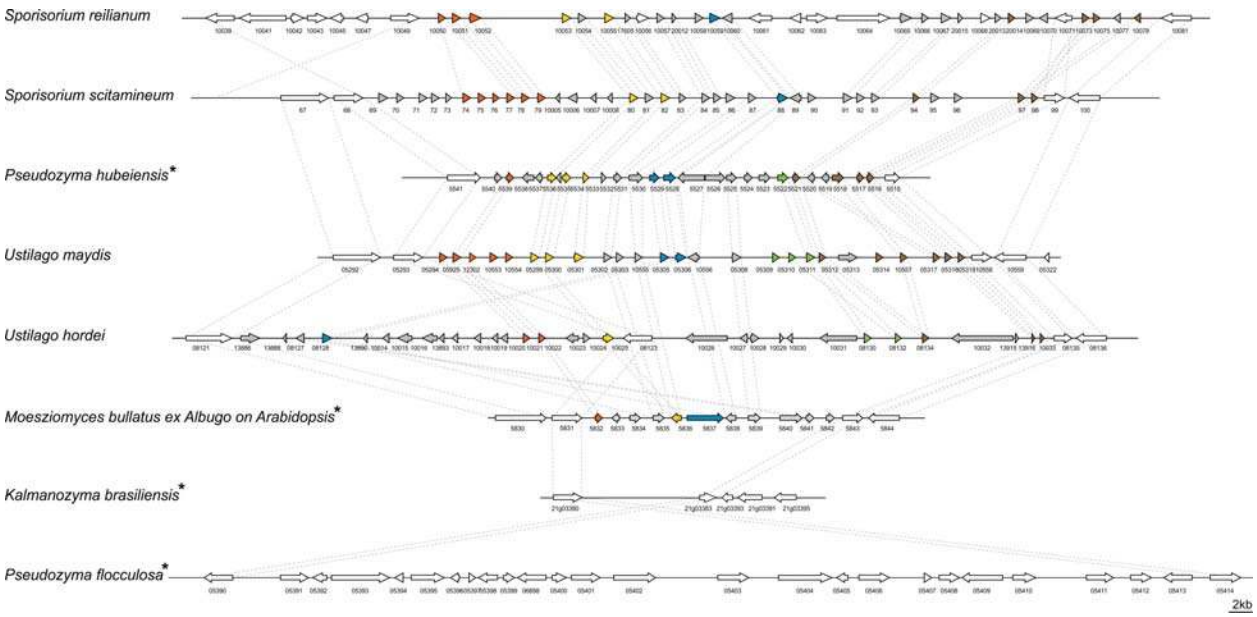

Figure 4: Structure of the largest virulence cluster (Cluster 19A) in pathogenic smut fungi and anamorphic smut yeasts (marked with*). Colors indicate genes with homology to each other: Related gene families are indicated in orange, yellow, blue, green and brown, whereas unique effector genes are shown in grey. Genes encoding proteins without a secretion signal are shown in white (24).

Figure 5

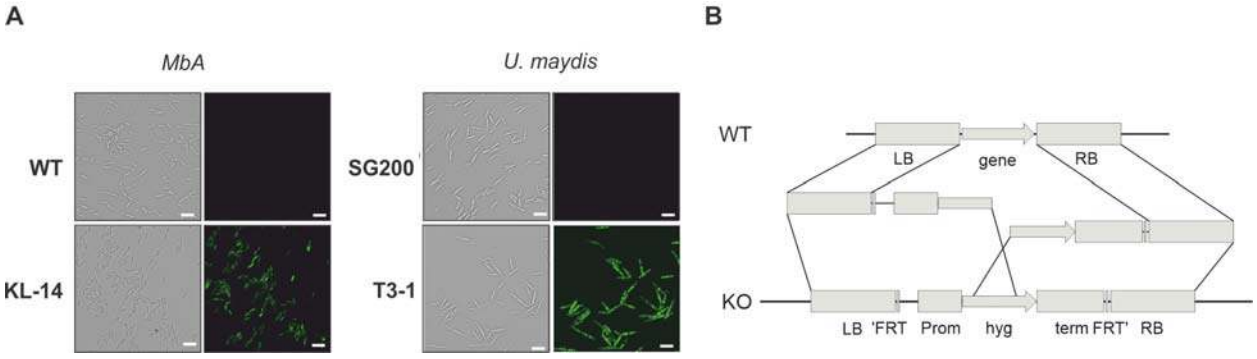

Figure 5: Genetic transformation of *MbA*. (A) Stable transformants that express cytosolic GFP could be obtained by generating protoplasts with Glucanex and ectopically integrating linear DNA-fragments into the genome via PEG-mediated transformation. (B) Overview of the split-marker approach that was used to generate deletion mutants via homologous recombination.

Figure 6

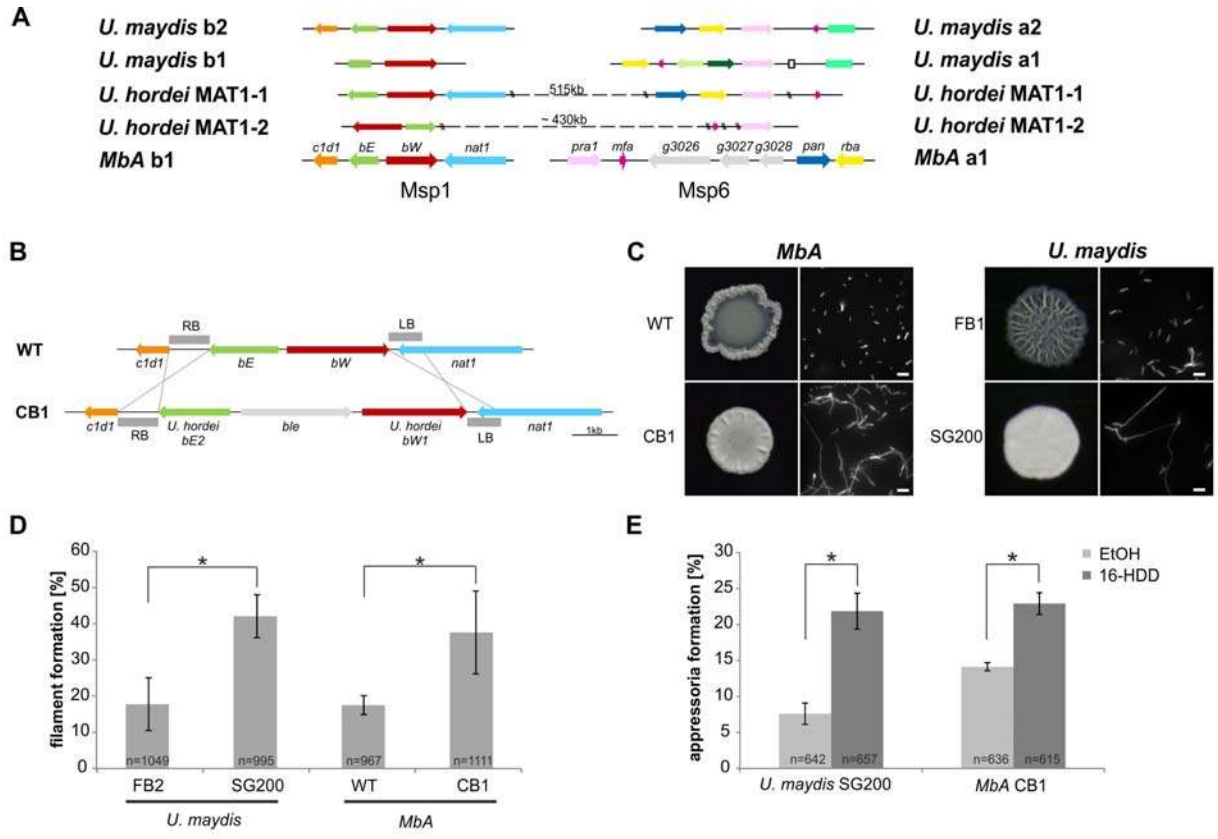

Figure 6: The self-compatible *MbA* strain CB1 (A) *MbA* mating type genes, unlike the ones of *U. hordei*, can be found on two different chromosomes similar to the tetrapolar mating type system of *U. maydis*. (B) To generate a self-compatible strain (CB1), the b-mating genes of *U.hordei* were integrated at the native *MbA b*-locus. (C) Unlike the *MbA* wild type strain (top left), strain CB1 (bottom left) shows a fluffy phenotype on charcoal plates and filamentous growth. *U. maydis* haploid F1 strain (top right) and self-compatible SG200 strain (bottom right) were used as negative and positive control, respectively. (D,E) Induction of filamentation and appressoria formation in strain CB1 was studied in three independent experiments. For this around 1000 cells for filament formation and around 600 cells for appressoria formation were analyzed and error bars indicate standard error. After incubation on a hydrophobic surface, both, filament and appressoria formation in strain CB1, were significantly different (* Chi-Square Test for Independence – α = 0,0001) when compared to *MbA* wild type and similar to the level of the self-compatible *U. maydis* strain SG00. *U. maydis* haploid F2 strain was used as negative control (18). Scale bar: 20µm. 16-HDD: 16-Hydroxyhexadecanoic acid.

Figure 7

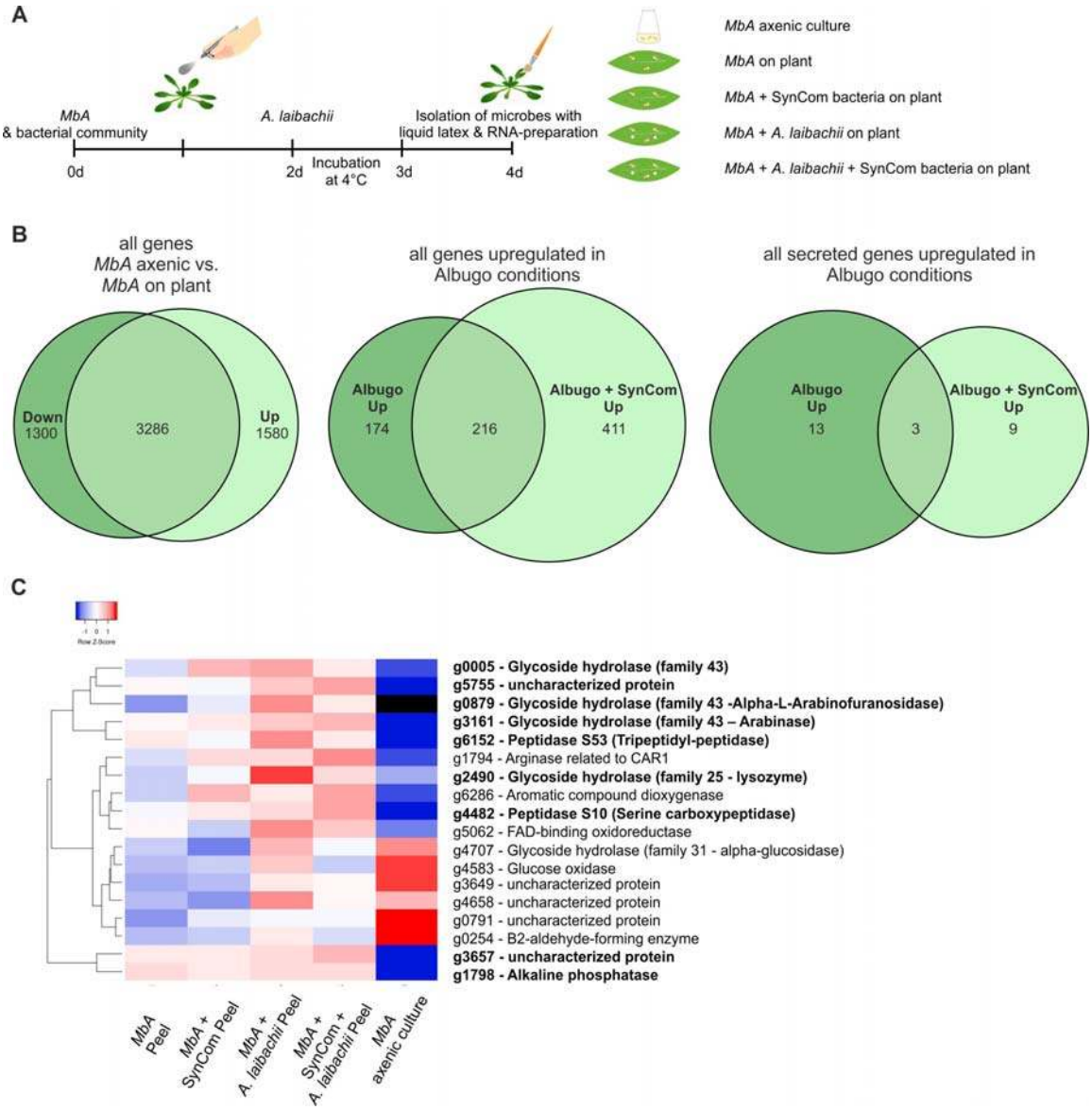

Figure 7: Transcriptome analysis of *MbA* (A) Experimental setup used for the transcriptomic (RNA-Sequencing) analysis in *MbA*. (B) Venn diagrams showing differential regulated *MbA* genes after spraying of haploid cells onto the *A. thaliana* leaf surface. A total number of 801 genes were upregulated in response to *A. laibachii* in presence and absence of bacterial SynCom. 216 of the 801 genes were upregulated in both conditions. (C) Hierarchical clustering of the 27 *A. laibachii* - induced *MbA* genes that are predicted to encode secreted proteins. Of these genes, nine were selected as candidate microbe-microbe effector genes, based on their transcriptional upregulation and prediction to encode for extracellularly localized proteins.

Figure 8

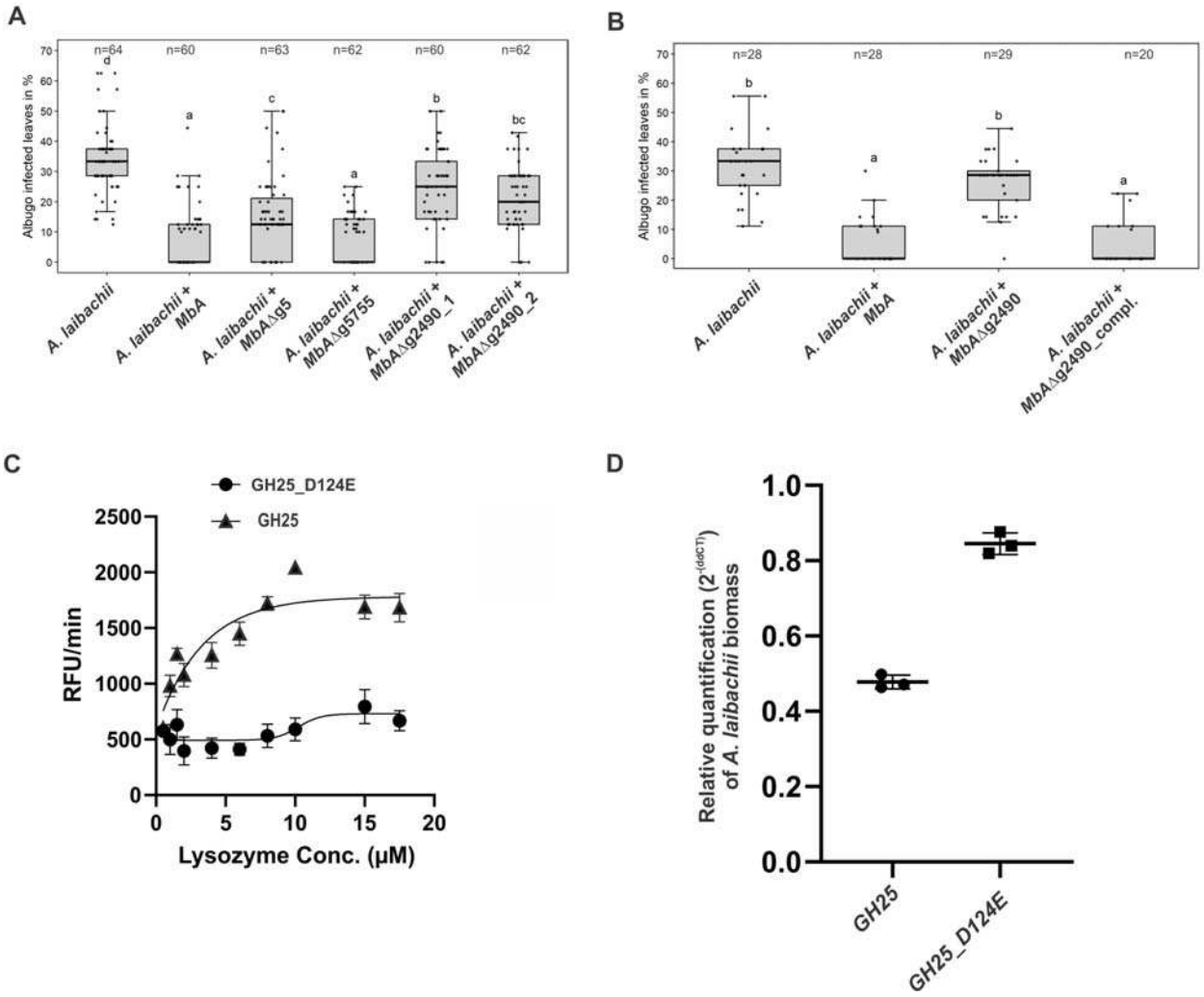

Figure 8: A reverse-genetic approach to identify the *MbA* gene which is responsible for the suppression of *A. laibachii* infection. (A) Three candidate microbe-microbe effector genes (*g5*, *g5755* &*g2490*) were deleted in *MbA* and deletion strains were individually inoculated on *A. thaliana* together with *A. laibachii*. Inoculation of two independent *g2490 null* strains *(Δg2490_1; Δg2490_2)* resulted in significant and almost complete loss the biocontrol activity of *MbA*. While deletion of g5 resulted in a marginal reduction of disease symptoms at 14 days post infection, deletion of g5755 had no effect on *A. laibachii.* (B) Genetic complementation of the *g2490* deletion restores the biocontrol activity to wild type levels. Infections in (A) were performed in six, in (B) in three individual replicates. In each replicate 12 plants were infected. N indicates the number of infected plants that were scored for symptoms. Different letters indicate significant differences (P values < 0.05; ANOVA model for pairwise comparison with Tukey's HSD test). (C) Detection of lysozyme. Increasing concentrations of purified MbA_GH25 and MbA_GH25(D124E)

were incubated with the DQ lysozyme substrate for an hour at 37 ˚C. The fluorescence was recorded every minute in a fluorescence microplate reader using excitation/emission of 485/530 nm. Finally, Relative Fluorescence Unit (RFU)/ min was calculated for each concentration and plotted on the graph. Each data point represents three technical replicates and three independent biological replicates as indicated by the Standard Error Measurement (SEM) bars. An unpaired t-test was performed for the active GH25 and Mutant_GH25 sets giving the p-value of <0.0001; and R squared value of 77.24%. (D) Relative quantification of *A. laibachii* biomass in response to MbA_GH25 (active and mutant) treatment via qPCR. The Oomycete internal transcribed spacer (ITS) 5.8s, was normalized to *A. thaliana* EF1-α gene to quantify the amount of *A. laibachii* DNA in the samples, ten days post infection. Then relative biomass was calculated comparing control sets (Only Albugo) with *A. laibachii* treated with GH25 and *A. laibachii* treated with Mutant_GH25 by ddCT method. Unpaired t-test between GH25 and Mutant_GH25 sets gave a p-value of <0.0001 and an R-squared value of 98.88%.